Towards a satellite – in situ hybrid estimate for organic aerosol abundance

Jin Liao[1,2], Thomas F. Hanisco[1], Glenn M. Wolfe[1,3], Jason St. Clair[1,3], Jose L. Jimenez[4,5], Pedro Campuzano-Jost[4,5], Benjamin A. Nault[4,5], Alan Fried[6], Eloise A. Marais[7], Gonzalo Gonzalez Abad[8], Kelly Chance[8], Hiren T. Jethva[1,2], Thomas B. Ryerson[9], Carsten Warneke[9,5], Armin Wisthaler[10,11]

[1]Atmospheric Chemistry and Dynamic Laboratory, NASA Goddard Space Flight Center, Greenbelt, MD, USA
[2]Universities Space Research Association, GESTAR, Columbia, MD, USA
[3]University of Maryland Baltimore County, Joint Center for Earth Systems Technology, Baltimore, MD, USA
[4]Department of Chemistry, University of Colorado, Boulder, Colorado, USA
[5]Cooperative Institute for Research in the Environmental Sciences, University of Colorado, Boulder, Colorado, USA
[6]Department of Atmospheric and Oceanic Sciences, University of Colorado Boulder, Boulder, Colorado, USA
[7]School of Geography, Earth and Environmental Sciences, University of Birmingham, UK
[8]Harvard-Smithsonian Center for Astrophysics, Cambridge, Massachusetts, USA
[9]NOAA Earth System Research Laboratory (ESRL), Chemical Sciences Division, Boulder, CO, USA
[10]Department of Chemistry, University of Oslo, Oslo, Norway
[11]Institute for Ion Physics and Applied Physics, University of Innsbruck, Innsbruck, Austria

Correspondence email: jin.liao@nasa.gov

Atmospheric
Chemistry
and Physics
Discussions

Abstract

30

31 Organic aerosol (OA) is one of the main components of the global particulate burden and

32 intimately links natural and anthropogenic emissions with air quality and climate. It is

33 challenging to accurately represent OA in global models. Direct quantification of global

34 OA abundance is not possible with current remote sensing technology; however, it may

35 be possible to exploit correlations of OA with remotely observable quantities to infer OA

36 spatiotemporal variability. In particular, formaldehyde (HCHO) and OA share common

37 sources via both primary emissions and secondary production from oxidation of volatile

38 organic compounds (VOCs). We examine OA-HCHO correlations using data from

39 summer-time airborne campaigns investigating biogenic (NASA SEAC^{4}RS and DC3),

40 biomass burning (NASA SEAC^{4}RS) and anthropogenic conditions (NOAA CalNex and

41 NASA KORUS-AQ). In situ OA correlates well with HCHO (r = 0.59 − 0.97) but the

42 slope and intercept of this relationship vary with chemical regime. For biogenic and

43 anthropogenic regions, the OA-vs-HCHO slope is higher in low NO_x conditions, where

44 HCHO yields are lower and aerosol yields are likely higher. The OA-vs-HCHO slope of

45 wild fires is more than 9 times higher than that associated with biogenic and

46 anthropogenic sources. An estimate of near-surface OA is derived by combining

47 observed in situ relationships with HCHO column retrievals from NASA's Ozone

48 Monitoring Instrument (OMI). We evaluate this OA estimate against OA observations

49 from the US EPA IMPROVE network and simulated OA from the GEOS-Chem global

50 chemical transport model. The OA estimate compares well with IMPROVE data obtained

51 over summer months (e.g. slope = 0.62, r = 0.56 for August 2013), comparable to

52 intensively validated GEOS-Chem performance (e.g. slope = 0.57, r = 0.56) and superior

53 to the correlation with satellite-derived total aerosol extinction (r = 0.41). Improving the

54 detection limit of satellite HCHO and expanding in situ airborne HCHO and OA

55 coverage in future missions will improve the quality and spatiotemporal coverage of this

56 OA estimate, potentially enabling constraints on the global OA distribution.

Atmospheric
Chemistry
and Physics
Discussions

1. Introduction

59   Aerosols are the largest source of uncertainty in climate radiative forcing (IPCC 2013;

60   Carslaw et al., 2013) and also decrease atmospheric visibility and impact human health

61   (Pope 2002). Organic aerosols (OA) comprise a large portion (~50%) of submicron

62   aerosols (Jimenez et al., 2009; Murphy et al., 2006; Shrivastava et al., 2017), and this

63   fraction will grow with continued decline in SO_2 emissions (Attwood et al., 2014; Marais

64   et al., 2017; Ridley et al., 2018). In addition, OA affect cloud formation and climate

65   radiative forcing such as the inclusion of phase-separation effects from organic material

66   into cloud droplet activation thermodynamics in climate models can lead to important

67   changes in cloud condensation nuclei (CCN) concentrations (Ovadnevaite et al., 2017).

68   OA components also have adverse health effects (e.g. Walgraeve et al., 2010) and

69   contribute significantly to regional severe haze events (e.g. Hayes et al., 2013). Finally,

70   because the response of temperature to changes in climate forcing is non-linear (Taylor

71   and Penner, 1994) and the forcing by aerosols has strong regional character (Kiehl and

72   Briegleb, 1993), it is necessary to separate out different climate forcing components to

73   accurately forecast the climate response to changes in forcing.

74

75   It is challenging to accurately represent OA in global models. Chemical transport models

76   (CTMs) often under-predict OA (e.g., more than 2 times less near the ground) compared

77   to observations, and model-to-model variability can exceed a factor of 100 in the free

78   troposphere (Tsigaridis et al., 2014; Heald et al., 2008; Heald et al., 2011). Fully explicit

79   mechanisms (e.g. Lee-Taylor et al., 2015) attempt to capture the full OA chemical

80   formation mechanisms, but many reaction rate constants and yields lack laboratory

Atmospheric
Chemistry
and Physics
Discussions

Open Access

EGU

81   validation. In addition, it is too computationally expensive to apply these mechanisms to

82   OA formation in global CTMs at a useful resolution. For computational efficiency, 3-D

83   models such as GEOS-Chem include direct emissions of primary OA (POA) and either

84   represents secondary OA (SOA) formation by lumping SOA products according to

85   similar hydrocarbon classes (Kim et al., 2015) or based on the volatility of the oxidation

86   products (Pye et al., 2010). Marais et al. (2016) applied an aqueous phase mechanism for

87   SOA formation from isoprene in GEOS-Chem to reasonably simulate isoprene SOA in

88   the southeast US, but this is only one location and it is likely that isoprene SOA is not the

89   dominant source of SOA in summer (Hu et al., 2015; Zhang et al., 2018). Accurate

90   emission inventories are also needed to correctly represent volatile organic compounds

91   (VOCs) and NO_x ($NO_x = NO + NO_2$) inputs, and these often have biases compared to

92   observational constraints (Kaiser et al., 2018, Travis et al., 2016, Anderson et al., 2014;

93   McDonald et al., 2018).

94

95   A quantitative measure of OA from space would be very helpful for verifying emissions

96   and aerosol processes in models. However, direct measurements of OA from space are

97   currently unavailable. Aerosol optical depth (AOD) measured by satellite sensors

98   provides a coarse but global picture of total aerosol distributions. MISR provides aerosol

99   property information such as size, shape and absorbing properties, which allows

100   retrieving AOD of a subset of aerosols when AOD is above a certain threshold (Kahn and

101   Gaitley, 2015). Classification algorithms have been developed to speciate different

102   aerosol types such as OA based on AOD, extinction Angstrom exponent, UV Aerosol

103   Index, and trace gas columns from satellite instruments (de Vries et al., 2015).

Atmospheric
Chemistry
and Physics
Discussions

104

105   Formaldehyde (HCHO) is one of the few VOCs that can be directly observed from space.

106   Sources emitting POA (e.g., biomass burning (BB)) often simultaneously release VOCs.

107   HCHO and SOA are also both produced from emitted VOCs. VOCs, as well as semi- and

108   intermediate- volatility organic compounds (S/IVOCs), are oxidized by hydroxyl radicals

109   (OH) to form peroxy radicals (RO_2), which then react with NO, RO_2, hydroperoxy

110   radicals (HO_2) or isomerize. These oxidation processes produce HCHO and oxidized

111   organic compounds with low volatility that condense to form SOA (Robinson et al.,

112   2007; Ziemann and Atkinson, 2012). The yield of HCHO and SOA from hydrocarbon

113   oxidation varies, depending on the VOC precursors, oxidants (OH, O_3 and NO_3), RO_2

114   reaction pathway (e.g. NO levels), and pre-existing aerosol abundance and properties

115   (Wolfe et al., 2016; Pye et al., 2010; Marais et al., 2016 and 2017; Xu et al., 2016).

116   Although the lifetime of HCHO (1-3 hrs) is shorter than OA (1 week), HCHO continues

117   to form from slower reacting VOCs, as well as from the oxidation of later generation

118   products. Observations across megacities around the world show that OA formation in

119   polluted/urban area happens over about 1 day (e.g. DeCarlo et al., 2010; Hodzic and

120   Jimenez, 2010; Hayes et al., 2013; 2015), and HCHO is also significantly formed over

121   this timescale (Nault et al., in preparation). Veefkind et al. (2011) found that satellite

122   AOD correlated with HCHO over the summertime Southeast US, BB regions, and

123   Southeast Asian industrialized regions. This also suggests that OA, a major contributor to

124   AOD in the above cases (Jimenez et al., 2009), and HCHO share common emission

125   sources and photochemical processes. Marais et al. (2016) further used the relationship

Atmospheric
Chemistry
and Physics
Discussions

126   between aircraft OA and satellite HCHO to evaluate GEOS-Chem representation of SOA

127   mass yields from biogenic isoprene in the Southeast US.

128

129   We present an OA surface mass concentration estimate (OA estimate) derived from a

130   combination of satellite HCHO column observations and in situ OA and HCHO

131   relationships. The detection limit of satellite HCHO column observations limit the quality

132   of OA estimate, thus we are focusing on summer time when HCHO levels are high. The

133   OA estimate is evaluated against OA measurements at ground sites. A 3-D model GEOS-

134   Chem OA simulation is also shown for comparison.

135

136   **2. Methods**

137   **2.1 In situ airborne observations**

138   Figure 1 shows flight tracks of field campaigns used in the current study. The Studies of

139   Emissions, Atmospheric Composition, Clouds and Climate Coupling by Regional

140   Surveys (SEAC[4]RS) mission (Toon et al., 2016) covered the continental US with a focus

141   on the southeast US in August-September 2013. The Deep Convective Clouds &

142   Chemistry Experiment (DC3) (Barth et al., 2015) surveyed the central and southeast US

143   in May-June 2012 while targeting isolated deep convective thunderstorms and mesoscale

144   convective systems. The California Research at the Nexus of Air Quality and Climate

145   Change (CalNex) (Ryerson et al., 2013) investigated the California region in May-June

146   2010, targeting the Los Angeles (LA) Basin and Central Valley. The Korea-United States

147   Air Quality Study (KORUS-AQ) studied South Korean air quality, including sampling

148   many large urban areas in South Korea and continental Asian outflow over the West Sea,

Atmospheric
Chemistry
and Physics
Discussions

149   in May-June 2016 (https://www-air.larc.nasa.gov/missions/korus-aq/). KORUS-AQ only

150   includes data with longitude < 133° E to exclude the transit from US because it targeted

151   South Korea and the nearby region. These field campaigns were selected as they had

152   recent high-quality in situ HCHO and OA data measured with state-of-the-art instruments

153   and studied summertime regional tropospheric chemical composition.

154

155   In situ airborne HCHO observations were acquired by multiple instruments. The DC3

156   NASA DC-8 payloads featured two HCHO measurements: the NASA In Situ Airborne

157   Formaldehyde (ISAF) (Cazorla et al., 2015) and the Difference Frequency Generation

158   Absorption Spectrometer (DFGAS) (Weibring et al., 2006). The SEAC^{4}RS NASA DC-8

159   payloads also featured two HCHO measurements: the NASA ISAF and the Compact

160   Atmospheric Multispecies Spectrometer (CAMS) (Richter et al., 2015). HCHO

161   measurements from ISAF were found to be in good agreement with CAMS, with a

162   correlation coefficient of 0.99 and a slope of 1.10 (Zhu et al., 2016). Because ISAF has

163   higher data density, we used ISAF HCHO data for DC3 and SEAC^{4}RS. During KORUS-

164   AQ, CAMS was the only HCHO instrument onboard the DC-8. In CalNex a proton

165   transfer reaction mass spectrometer (PTRMS) (Warneke et al., 2011) was used to

166   measure HCHO on board the NOAA P3 aircraft.

167

168   In situ airborne OA from SEAC^{4}RS, DC3, and KORUS-AQ was measured by the

169   University of Colorado High-Resolution Time-of-Flight Aerosol Mass Spectrometer

170   (AMS, DeCarlo et al., 2006; Dunlea et al., 2009; Canagaratna et al., 2007; Jimenez et al.,

171   2016) and in situ airborne OA from CalNex was measured by the NOAA Compact Time-

Atmospheric
Chemistry
and Physics
Discussions

172   of-Flight Aerosol Mass Spectrometer (Drewnick et al., 2005; Canagaratna et al., 2007;

173   Bahreini et al., 2012). The OA measurements are from 1 min merge data and converted

174   from $\mu g \ sm^{-3}$ to $\mu g \ m^{-3}$ under local T & P for each data point.

175

176   Although NO modulates the RO_2 lifetime, and thus, the production of HCHO and SOA, it

177   cannot be directly observed via remote sensing. Instead, NO_2 can be directly observed in

178   space by satellites, and since NO_2 represents typically ~80% (e.g. SEAC[4]RS and

179   KORUS-AQ) of the boundary layer NO_x concentrations during the daytime, it can be

180   used as a surrogate for NO concentrations and oxidative conditions around the globe. In

181   situ airborne NO_2 was measured by the NOAA Chemiluminescence NO_yO_3 instrument

182   (Ryerson et al., 2001) during SEAC[4]RS and by University of Berkeley laser induced

183   fluorescence NO_2 instrument (Day et al., 2002) during KORUS-AQ.

184

185   **2.2 Ground-based OA measurements**

186   Ground-based OA measurements over the US are from the EPA Interagency Monitoring

187   of Protected Visual Environments (IMPROVE) (Malm et al., 1994; Solomon et al., 2014;

188   Hand et al., 2014; Hand et al., 2013; Malm et al., 2017) and Southeastern Aerosol

189   Research and Characterization (SEARCH) (Edgerton et al., 2006) networks. In the

190   IMPROVE network, aerosols were collected on quartz fiber filters and analyzed in the

191   lab by thermal optical reflectance for organic and elemental carbon. The data were

192   reported every three days from 1988 to 2014. Monthly averages were used for

193   comparison in this study. IMPROVE OA data over the southeast US (east of 70ºW) in

194   summertime were multiplied by a factor of 1.37 to correct for partial evaporation during

Atmospheric
Chemistry
and Physics
Discussions

Open Access

EGU

195   filter transport, following the recommendation of a comparison study with SEARCH

196   organic carbon (OC) measurements (Kim et al., 2015; Hand et al., 2013). Although

197   IMPROVE OA corrected for evaporation has potential uncertainties with the constant

198   scaling factor, the IMPROVE measurements have high spatial coverage. SEARCH

199   network (Edgerton et al., 2006; Hidy et al., 2014) OC is determined by the difference

200   between total carbon (TC) detected by a tapered element oscillating microbalance

201   (TEOM) and black carbon (BC) measured by an in situ Thermal Optical instrument. This

202   allows real-time measurement of OC and prevents evaporation during filter transport.

203   Although the SEARCH network only has 5 sites available, we also use observations from

204   this network due to their high accuracy. The IMPROVE and SEARCH network OC

205   measurements were converted to OA by multiplying by a factor of 2.1 based on ground

206   and aircraft observations (Pye et al., 2017; Schroder et al., 2018).

207

208   **2.3 Satellite measurements**

209   Satellite HCHO column observations are derived from the NASA's Ozone Monitoring

210   Instrument (OMI), a UV/Vis nadir solar backscatter spectrometer on the Aura satellite

211   (Levelt et al., 2006). Aura overpasses the equator at 1:30 pm local time, daily. Here we

212   use the OMI HCHO version 2.0 (collection 3) retrieval (Gonzalez Abad et al., 2015) from

213   the Smithsonian Astrophysical Observatory (SAO). Satellite data for HCHO columns

214   were subjected to data quality filters: 1) solar zenith angle lower than 70°, 2) cloud

215   fraction less than 40%, and 3) main quality flag and the xtrackquality flag both equal to

216   zero

217   (https://www.cfa.harvard.edu/atmosphere/Instruments/OMI/PGEReleases/READMEs/O

Atmospheric
Chemistry
and Physics
Discussions
Open Access
EGU

218   MHCHO_README_v3.0.pdf). The monthly average HCHO columns were also

219   weighted by the column uncertainties of the pixels. The HCHO retrieval used a priori

220   profiles without aerosol information from the GEOS-Chem model (Gonzalez Abad et al.,

221   2015). Satellite NO_2 column observations are also derived from NASA's OMI level 3

222   data, archived at hbps://disc.sci.gsfc.nasa.gov as "OMI-Aura_L3-OMNO2d" (Lamsal et

223   al., 2014).

224   Satellite AOD observations were acquired from the Moderate Resolution Imaging

225   Spectroradiometer (MODIS) onboard the Aqua satellite, using overpasses at about 1:30

226   pm   local   time.   Here,   we   use   collection   06   (MYD04_L2,

227   hbps://ladsweb.nascom.nasa.gov/), retrieved using the Dark Target (DT) and Deep Blue

228   (DB) algorithms (Levy et al., 2015).

229

230

231   **2.4 GEOS-Chem**

232   We used GEOS-Chem (v9-02) at 2° × 2.5° with 47 vertical layers to simulate HCHO and

233   OA globally, the same as that in Marais et al. (2016). GEOS-Chem is driven with

234   meteorological fields from the NASA Global Modeling and Assimilation Office

235   (GMAO). The OA simulation includes POA from fires and anthropogenic activity and

236   SOA from the volatility-based reversible partitioning scheme (VBS) of Pye et al. (2010)

237   for anthropogenic, fire, and monoterpene sources, and an irreversible aqueous-phase

238   reactive uptake mechanism for isoprene. The aqueous-phase mechanism is coupled to

239   gas-phase isoprene chemistry and has been extensively validated using surface and

240   aircraft observations of isoprene SOA components in the Southeast US (Marais et al.,

241 2016). The model is driven with Goddard Earth Observing System – Forward Processing

242 (GEOS-FP) meteorology for 2013 and sampled along the SEAC[4]RS (2013) and KORUS-

243 AQ (2016) flight tracks. The model is also run with 10% decrease in biomass burning,

244 biogenic, or anthropogenic emissions as sensitivity test to evaluate the contributions of

245 different sources to OA and HCHO budget. Model monthly mean surface layer OA and

246 total column formaldehyde are obtained around the OMI overpass time (12:00-15:00

247 local time) for 2008-2013 using MERRA Modern-Era Retrospective analysis for

248 Research and Applications (MERRA) meteorology, as GEOS-FP is only available from

249 2012. This is compared to the OA estimate derived from satellite HCHO.

250

251 Global isoprene emissions are used to calculate an isoprene and NO_2 dependent OA

252 estimate. Global isoprene emissions are from the Model of Emissions of Gases and

253 Aerosols from Nature version 2.1 (Guenther et al., 2006) as implemented in GEOS-Chem

254 and driven with MERRA (MEGAN-MERRA).

255

256 **2.5 Estimation of surface organic aerosol mass concentrations**

257 An estimate for surface OA mass concentration is calculated based on a simple linear

258 transformation.

259 $\varepsilon(i) = \Omega_{HCHO}(i)\eta(i)\alpha(i) + \beta(i)$ Eq. (1)

260 Here, $\varepsilon(i)$ is the OA estimate for grid cell i (μg m^{-3}), $\Omega_{HCHO}(i)$ is the OMI HCHO column

261 density (molec cm^{-2}) in each 0.25°×0.25° grid cell (similar resolution to OMI HCHO

262 nadir pixel data), $\eta(i)$ is the ratio of midday surface layer (~140 m) HCHO concentrations

263 (molec cm^{-3}) to column concentrations (molec cm^{-2}) from GEOS-Chem, and $\alpha(i)$ and

264    $\beta(i)$ are the slope and intercept of a linear regression between OA and HCHO from low

265   altitude (<1 km) airborne in situ measurements. The in situ to column conversion factor

266    $\eta(i)$ is similar to that used by Zhu et al. (2017) to convert HCHO columns into surface

267   concentrations. $\eta(i)$ is derived from GEOS-Chem (v9-02), which includes updated

268   isoprene scheme for OA and is the next version of the model (v9-01-03) for a priori

269   profiles used in SAO satellite HCHO retrievals. The detailed information about η is

270   provided in Sect. 5.

271

272   **2.6 Aerosol extinction from satellite measurements**

273   Currently remote sensing observes aerosols by quantifying AOD. The MISR satellite

274   instrument can estimate the fraction of OA relative to total AOD, due to constraints on

275   size range, shape and absorbing properties, but cannot distinguish OA from other

276   submicron aerosol compounds such as sulfate and nitrate and also requires AOD above

277   0.1. Moreover, OA account for a large and relatively constant fraction of submicron

278   aerosols in the Southeast US (Kim et al., 2015; Wagner et al., 2015). Therefore, AOD

279   was converted to extinction to represent OA for comparison.

280    $A_{ext} = \text{AOD}(i)\delta(i)$ Eq. (2)

281   where AOD(i) is aerosol optical depth from MODIS (see Sect. 2.3) in each 0.25°×0.25°

282   grid cell, and $\delta(i)$ (m^{-1}) is the ratio of surface layer OA concentrations ($\mu g \ m^{-3}$) to column

283   OA concentrations ($\mu g \ m^{-2}$) from GEOS-Chem multiplied by $10^6 \ Mm^{-1}/m^{-1}$. The shape

284   of average vertical profile of OA was very close to that of total aerosol mass (Wagner et

285   al., 2015).

286

3. In situ OA and HCHO relationship

Although OA and HCHO share common VOC emission sources and photochemical processes, their production rates from different emission sources and photochemical conditions vary, as do their loss rates. The following section discusses the main factors that modulate OA-HCHO relationships.

3.1 Regional and Source-Driven Variability

For all regions and/or sources investigated, in situ OA and HCHO are well correlated. A scatter plot of in situ OA vs. HCHO at low altitudes (<1 km) from a number of field campaigns (SEAC[4]RS, DC3, CalNex, and KORUS-AQ) is displayed in Fig. 2. The slope, intercept and correlation coefficient are provided in Table 1. SEAC[4]RS, DC3, and CalNex excluded BB data when acetonitrile > 200 pptv (Hudson et al., 2004). KORUS-AQ used a BB filter with higher acetonitrile (>500 pptv) because the air masses with moderate acetonitrile enhancement (200-500 pptv) were actually from anthropogenic emissions. This attribution is based on high levels of acetonitrile detected downwind of Seoul and west coastal petrochemical facilities, the slope between acetonitrile and CO being to urban emissions (Warneke et al., 2006), and the concentrations of anthropogenic tracer $CHCl_3$ being high (Warneke et al., 2006). Similar to acetonitrile, another common BB tracer hydrogen cyanide (HCN) was also enhanced in these air masses. BB data (acetonitrile > 200 pptv) for SEAC[4]RS were analyzed separately and are inset in Fig. 2. Although all CalNex data had a tight correlation, we only included the flight data near LA basin to target the area strongly influenced by anthropogenic emissions. In general,

Atmospheric
Chemistry
and Physics
Discussions

309   the correlation coefficients between in situ OA and HCHO were strong (r = 0.59 −0.97)

310   (Table 1).

311

312   The variety in OA-HCHO regression coefficients among different campaigns reflects the

313   regional and/or source-driven OA-HCHO variability. Considering only the non-biomass

314   burning (non-BB) air masses sampled, OA and HCHO had the tightest correlation for

315   CalNex, because CalNex focused on the LA area (shown in Fig. 2) and Central Valley

316   while SEAC[4]RS and DC3 covered a larger area with a potentially larger variety of

317   sources and chemical conditions. Although SEAC[4]RS and DC3 both sampled the

318   continental US, SEAC[4]RS had more spatial coverage and sampled more air masses at low

319   altitudes, while DC3 was designed to sample convective outflow air masses and had more

320   data at high altitudes. Although KORUS-AQ covered a much smaller area compared to

321   SEAC[4]RS, KORUS-AQ data also had a large spread, which may be due to the

322   complicated South Korean anthropogenic sources mixed with transported air masses

323   (mainly from China) and possibly biogenic sources. OA exhibits a tight correlation with

324   HCHO for both wildfires and agricultural fires. This is because the production of HCHO

325   and OA is much higher in BB air masses compared to background. This may also suggest

326   that the emissions of OA and HCHO in these air masses are relatively constant. More

327   intensive fire sampling is needed to probe the correlation between OA and HCHO across

328   fuel types and environmental conditions.

329

330   The different slopes of OA-HCHO among different campaigns also reflect the regional or

331   source-driven OA-HCHO variability. The slopes of OA vs. HCHO were more similar

332   between DC3 and SEAC[4]RS. The slope of OA vs. HCHO was higher for South Korea

333   (KORUS-AQ), which is dominated by anthropogenic emissions compared to the

334   biogenic-dominated emission in the Southeast US (SEAC[4]RS and DC3). The high OA air

335   masses also had high acetonitrile during KORUS-AQ. The slope of OA-HCHO for

336   California LA basin, dominated by anthropogenic emissions, was also not as high as

337   South Korea. The potential difference in the anthropogenic emissions mix could

338   contribute to the different OA-HCHO slopes from US LA region and South Korea

339   anthropogenic sources (Baker et al., 2007; Na et al., 2005; Na et al., 2002). The slopes of

340   OA vs. HCHO for BB air masses were higher than for anthropogenic and biogenic

341   sources. This is consistent with high POA emission in BB conditions (Heald et al., 2008;

342   Lamarque et al., 2010; Cubison et al., 2011), despite low addition of mass due to SOA

343   formation (Cubison et al., 2011; Shrivastava et al., 2017). The slope of OA to HCHO was

344   higher for wildfires than agricultural fires. This may indicate that more OA is emitted in

345   wildfires which often have higher intensity than agricultural fires (Liu et al., 2017;

346   Forrister et al., 2015).   As SEAC[4]RS had the largest geographic coverage for low altitude

347   data over US, the campaign average slope of OA vs. HCHO was used to represent the US

348   region in summer, except large cities where CalNex LA Basin data were used.

349

350

351   **3.2 Dependence on NO$_x$ and VOCs speciation**

352   Biogenic and anthropogenic VOCs are oxidized by atmospheric oxidants (e.g. OH as the

353   dominant oxidant) to form RO$_2$. HCHO is produced from the reactions of RO$_2$ with HO$_2$

354   or NO, with RO$_2$+NO typically producing more HCHO than RO$_2$ + HO$_2$ (e.g. Wolfe et

355   al., 2016). RO$_2$ can react with HO$_2$, NO, or isomerize to form oxidized organic

Atmospheric
Chemistry
and Physics
Discussions

356   compounds with high molecular weight and low volatility, which condense on existing

357   particles to form SOA.   The products of RO_2 + NO tend to fragment instead of

358   functionalize and often lead to higher volatility compounds (e.g. HCHO) and thus less

359   SOA formation compared to the products of $RO_2 + HO_2$ (Kroll et al., 2006; Worton et al.,

360   2013). Therefore, with the same VOC, we expect more HCHO and less OA formed at

361   high NO conditions and vice versa. As mentioned before, NO_2 instead of NO is easily

362   measured from space and NO_2 typically is ~80% of NO_x in the boundary layer during the

363   day. Therefore, NO_2 is used as a surrogate for the NO levels influencing OA and HCHO

364   production.   The yields of HCHO and SOA also depend on VOC speciation (e.g. Lee et

365   al., 2006).   Specifically, isoprene has a higher yield of HCHO than most non-alkene

366   VOCs (Dufour et al., 2009).

367

368   A scatter plot of OA vs. HCHO for SEAC[4]RS low altitude data is shown in Fig. 3(a). The

369   data are color-coded by the product of in-situ isoprene and NO_2, attempting to capture

370   time periods strongly influenced by oxidation products of isoprene at high NO

371   conditions. No obvious trends are evident when the data are instead color coded by NO_2

372   or isoprene only. This may be because isoprene (biogenic source) and NO_2

373   (anthropogenic sources) are generally not co-located in the US (Yu et al., 2016) and

374   isoprene is the dominant source of HCHO compared to anthropogenic VOCs in the US

375   (e.g. Millet et al., 2008). This plot shows that, at high NO_2 and high isoprene conditions,

376   less OA was formed for each HCHO produced generally. This is consistent with high NO

377   and isoprene conditions promote HCHO formation over SOA formation. We also looked

378   at the dependence on peroxy acetyl nitrate (PAN), as PAN is a product of the photo

Atmospheric
Chemistry
and Physics
Discussions

379   oxidation of VOCs, including isoprene, in the presence of NO_2. The dependence on PAN

380   was not as clear as on the product of NO_2 and isoprene.

381

382   KORUS-AQ OA vs. HCHO, color-coded with NO_2, is plotted in Fig. 3(b). The OA /

383   HCHO ratio clearly decreased as NO_2 levels increased during KORUS-AQ, suggesting

384   that high NO conditions accelerated HCHO formation more than they did SOA

385   production.   Compared to SEAC4RS, the KORUS-AQ OA/HCHO ratio does not depend

386   on VOCs. This may be consistent with the dominant VOC being anthropogenic VOCs

387   that are co-located with NO sources. This may also suggest the anthropogenic VOCs

388   generally have a lower HCHO yield than does isoprene.

389

390

391   **4. Comparison of OA and HCHO relationship: in-situ vs. GEOS-Chem**

392   In situ OA vs. HCHO relationships from SEAC[4]RS low altitude non-BB (Fig. 4a),

393   KORUS-AQ low altitude (Fig. 4b), and SEAC[4]RS BB (Fig. 4c) air masses were

394   compared to GEOS-Chem model simulations (Fig. 4d-4f) sampling along the

395   corresponding flight tracks. Similar to the in situ data, GEOS-Chem model simulations

396   also found correlations between OA and HCHO for these three regions, especially for

397   SEAC[4]RS non-BB. GEOS-Chem was intensively validated with in situ measurements for

398   Southeast US (e.g. Marais et al., 2016; Kim et al., 2015). The ratios of the slopes between

399   OA and HCHO for the US (SEAC[4]RS), South Korea (KORUS-AQ), and wildfire cases

400   (SEAC[4]RS) from GEOS-Chem were 1:1.1:0.4, which was different from the in situ

401   measurements ratios of 1:1.4:13 (Table 1). GEOS-Chem could not capture any wild fires

Atmospheric
Chemistry
and Physics
Discussions

402   in US during SEAC^{4}RS, which is probably due to poor representation of BB emission

403   inventory for US wildfire and also the coarse grid in GEOS-Chem. GEOS-Chem also

404   significantly under predicted the slope of OA to HCHO for South Korea. We attribute

405   this to a likely underprediction of anthropogenic SOA, which was dominant in South

406   Korea, in GEOS-Chem (Schroder et al., 2018), as well as a different mix of OA and

407   HCHO sources in the US compared to South Korea and representation of these in GEOS-

408   Chem. Although GEOS-Chem contains isoprene chemistry with a focus on the Southeast

409   US (Marais et al. 2016), there is still room to improve the model especially for

410   anthropogenic and BB sources, as well as anthropogenic OA formation mechanisms. For

411   example, in the model biogenic sources are more important than anthropogenic sources

412   for the OA and HCHO budgets in South Korea , which is not the case from KORUS-AQ

413   in situ measurements. A 10% decrease of emissions from biogenic, anthropogenic and

414   BB sources results in a 6%, 3%, and 1% decrease in OA and 2%, 1%, and 0% decrease in

415   HCHO over South Korea in May 2016. However, the in situ airborne field campaign

416   KORUS-AQ found that OA and HCHO were higher near anthropogenic emission sources

417   compared to rural regions. The larger impact of biogenic sources compared to

418   anthropogenic sources on OA and HCHO in the model can be due to both low-biased

419   anthropogenic emission inventories and low-biased anthropogenic SOA. Improving

420   anthropogenic emissions inventories in the models can also bring model results closer to

421   observations. Improving anthropogenic SOA, such as implementation of the SIMPLE

422   model, in GEOS-Chem (Hodzic and Jimenez, 2011) can also improve the model results

423   compared to observations. Measurements or measurement-constrained estimation with

424   sufficient spatial and temporal coverage can help to narrow down the key factors (e.g.

Atmospheric
Chemistry
and Physics
Discussions

425   emission inventories or chemical schemes) in GEOS-Chem to better represent VOCs and

426   OA globally. Furthermore, we did also find that GEOS-Chem could not capture the

427   observed higher slope of OA to HCHO at high altitudes (not shown), which could be due

428   to issues such as transport, OA lifetime, and OA production.

429

430

431

432   **5. Relating satellite HCHO column to surface HCHO concentrations**

433   To utilize the derived in-situ OA and HCHO relationship, the satellite HCHO column

434   needs to be converted to surface HCHO concentrations. We used a vertical distribution

435   factor η (cm^{-1}) (Sect. 2.5), which is defined as the ratio of surface HCHO concentrations

436   (molec cm^{-3}) to HCHO column (molec cm^{-2}), to estimate surface HCHO concentrations

437   from satellite column measurements. Zhu et al. (2017) used the same vertical distribution

438   factor for their study. The use of this factor is justified by the fact that the derived surface

439   HCHO retained the spatial pattern of the satellite HCHO column and agreed with local

440   surface measurements of HCHO for a multi-year average (Zhu et al., 2017).

441

442   We also investigated the main factors affecting the variation of the vertical distribution

443   factor η. Because the factor is determined by HCHO vertical distributions, we examined

444   three typical normalized HCHO vertical distribution profiles with the highest, median and

445   lowest η values for the SEAC[4]RS field campaign (Fig. 5). GEOS-Chem can generally

446   capture the vertical profiles of measured HCHO. Boundary layer mixing height and

447   surface emission strength are the dominant factors in determining the fraction of HCHO

448   near the surface. We can see that higher boundary layer mixing height results in lower η

449   for southeast US profiles, where there are biogenic sources of HCHO from the surface

450   and HCHO has distinct concentration difference below and above the boundary layer.

451   However, there are exceptions, such as for the profiles over the ocean and the coastal

452   regions. Although the boundary layer is shallow in these regions, a large portion of

453   HCHO resides above the boundary layer, resulting in low η. In these cases, surface

454   emissions of HCHO or precursors are very small and therefore methane oxidation makes

455   a large contribution to the total HCHO column. High concentrations of HCHO (e.g., in

456   BB plumes) lofted by convection can also impact the vertical profile (Barth et al., 2015).

457   Overall, the source intensities and boundary layer mixing height mostly determined the

458   HCHO vertical profiles.

459

460   **6. Construction of the OA estimate**

461   **6.1 Variables to construct OA estimate**

462   As mentioned in Sect. 2.5, the OA estimate value in each grid cell is estimated from

463   satellite HCHO column observation by the linear Eq. (1). Satellite HCHO columns,

464   Ω_{HCHO}, are converted to surface HCHO concentrations by multiplying by the $\eta(i)$ factor.

465   Surface OA is then estimated by the derived surface HCHO concentrations and applying

466   the linear regression equation (slope $\alpha(i)$ and intercept $\beta(i)$) between in situ OA and

467   HCHO determined from in-situ aircraft field campaign data. The relationship between

468   OA and HCHO varies but previous sections demonstrated that we can quantify the

469   surface OA-HCHO relationship by their regions, sources and chemical conditions (e.g.,

470   NO_x levels). To test the impact of the chosen OA-HCHO relationship on the calculated

471   OA estimate, the OA estimate in the US was calculated using four different methods (see

472   Table 2).

473

474   **6.2 OA estimate over US**

475   The monthly average surface OA estimate over the US in August 2013 for case 1 (Sect.

476   6.1) is shown in Fig. 6(a). Because BB regions in the US are not covered by smoke

477   continuously during a period of time and it is challenging for satellite retrieval to separate

478   thick BB plumes and clouds without information on the time and location of the burning,

479   thick BB events (OMI UV Aerosol Index (UVAI) > 1.6) (Torres et al., 2007) were

480   excluded and shown as the blank (white) grid cells in Fig. 6(a). The same filter was also

481   applied to aerosol extinction and GEOS-Chem OA abundance. To evaluate the

482   representative quality of the OA estimate, OA estimate data were compared to the EPA

483   IMPROVE ground sites corrected-OA measurements over the US and SEARCH ground

484   sites OA measurements in the Southeast US (Sect. 2.2). The locations of IMPROVE and

485   SEARCH sites are displayed in Fig. 6(g) as small and large dots, respectively. The dot

486   color represents the average OA mass concentrations for August 2013.

487

488   The good correlation between the OA estimate and corrected IMPROVE network

489   measurements (Fig. 6(e)) indicates that the OA estimate generally captured the variation

490   of OA loading over the US. The correlation between the OA estimate and IMPROVE OA

491   measurements yielded a slope of 0.62, indicating that the OA estimate slightly

492   underestimated OA. Satellite HCHO data were measured in mid-day, in situ airborne OA

493   and HCHO were measured during the daytime and IMPROVE network organic carbon

Atmospheric
Chemistry
and Physics
Discussions

494   was collected day and night. Because ground OA in the Southeast US were observed to

495   have little diurnal variation (Xu et al., 2015; Hu et al., 2015), the different sampling time

496   of ground and airborne OA probably does not have a significant impact on the

497   comparison of OA estimate and IMPROVE OA. The difference in mid-day and daytime

498   HCHO concentrations is not prominent, depends on the location and may contribute to a

499   small bias to the mid-day OA estimate (DiGangi et al., 2012). This is probably due to

500   increased boundary layer height diluting the photochemical formation of HCHO in the

501   mid-day. Instead, the potential underestimation of HCHO from satellite retrieval (by

502   37%) (Zhu et al., 2016) compared to SEAC[4]RS may cause the low slope between the OA

503   estimate and IMPROVE OA according to Eq. (1). Also, the uncertainty in η estimated

504   from GEOS-Chem could have also contributed to the low slope between the OA estimate

505   and EPA ground site OA. Furthermore, the uncertainties in IMPROVE OA

506   measurements, such as using a correction factor to correct the partial evaporation across

507   all southeast US sites, and real variations on the OA/OC ratio, may also have contributed

508   to the discrepancies between the OA estimate and EPA IMRPOVE sites OA.

509

510   SEARCH OA data were also used to compare to the OA estimate. The correlation was

511   good for August 2013. Although the SEARCH network OA measurements have better

512   accuracy, the number of SEARCH sites is limited (5 sites). The correlation of OA

513   estimate and SEARCH OA varied dramatically 2008-2013 (Fig. S1). GEOS-Chem OA

514   does not correlate with SEARCH OA except for the year 2013 (Fig. S1). As the

515   IMPROVE network has more sites and spatial coverage, we use IMPROVE network data

516   as ground OA measurements for comparison in the remainder of the discussion.

Atmospheric
Chemistry
and Physics
Discussions

517

6.3 Comparison to aerosol extinction from AOD

519   To further evaluate the method of using satellite HCHO to derive an OA surface estimate,

520   satellite measurements of AOD were converted to extinction for comparison. Studies

521   showed that OA were a dominant component of aerosol mass and extinction during

522   SEAC[4]RS (Kim et al., 2015; Wagner et al., 2015) and the fractions of OA were relatively

523   constant (interdecile 62-74%) (Wagner et al., 2015). Therefore AOD variation is

524   expected to generally reflect the OA variation during SEAC[4]RS. Satellite measurements

525   from MISR can provide more aerosol property information to apportion total AOD to

526   AOD of a subset of aerosols with small to medium size and round shape, which can

527   better capture OA, when AOD is above 0.15 to 0.2 (Kahn and Gaitley, 2015; personal

528   communication with R. Kahn, 2018). Because MISR cannot distinguish OA and other

529   submicron aerosol components (e.g. sulfate and nitrate), the fractions of OA were

530   relatively constant, and AOD below 0.15 or 0.2 accounts for near half of the data over US

531   in August, 2013, we use total AOD to derive extinction for our comparison. The AOD-

532   derived extinction map is shown in Fig. 6(b), and the scatter plot of AOD-derived

533   extinction and EPA corrected OA is displayed in Fig. 6(f). The same filter of high AI was

534   also applied to AOD-derived extinction to remove BB plumes. Generally, the derived

535   aerosol extinction had a correlation with IMPROVE OA, but the correlation is not as

536   good as for the OA estimate with IMPROVE OA. This indicates that the OA estimate

537   derived from HCHO may be better than AOD at representing the concentrations of OA,

538   even for the regions where AOD is dominated by OA (Xu et al., 2015).

539

6.4 Comparison to GEOS-Chem OA

540

541 Surface OA over the US from a GEOS-Chem simulation for August 2013 is shown in

542 Fig. 6(c), and the scatter plot of GEOS-Chem OA with IMPROVE OA is in Fig. 6(g).

543 The GEOS-Chem simulation had a coarser resolution than satellite HCHO data. To be

544 comparable to the OA estimate, the scatter plot Fig. 6(g) used GEOS-Chem results for the

545 grid squares that overlap with individual IMPROVE sites. Compared to the OA estimate,

546 GEOS-Chem OA had a similar correlation coefficient with IMPROVE OA. Although the

547 GEOS-Chem OA plot appears more scattered, there are many GEOS-Chem data points

548 close to zero when IMPROVE OA was low, making the overall correlation coefficient

549 similar to that for the OA estimate. GEOS-Chem under predicted IMPROVE OA more

550 with a slope of 0.57 compared to the OA estimate. This is consistent with underprediction

551 of anthropogenic OA in Marais et al. (2016).

552

6.5 OA estimate with different OA-HCHO relationships

553

554 In general, OA estimate results from the four cases were similar. The OA proxies from

555 the four cases (Table 2) were compared to IMPROVE OA and the correlation coefficients

556 are shown in Fig. 7. Applying CalNex LA Basin in situ data (case 3) to bring down the

557 OA concentrations of LA resulted in a similar correlation. The uncertainties in

558 IMPROVE OA measurements may contribute to this. Including the NO_2–isoprene-

559 dependent OA and HCHO relationship (case 2) showed a similar (or slightly worse)

560 correlation between the OA estimate and IMPROVE OA. As the in situ data showed a

561 NO_2–isoprene-dependent OA and HCHO relationship, we attributed this to the

562 uncertainty of isoprene emissions from MEGAN or IMPROVE network measurements.

Atmospheric
Chemistry
and Physics
Discussions

563   Because separating large urban areas and other regions and applying a chemical region

564   dependent in situ OA and HCHO relationship did not improve the agreement between the

565   OA estimate and IMPROVE OA, we used the base case OA and HCHO relationship

566   (case 1) to derive the OA estimate (shown in Fig. 6).

567

568

569   **6.6 Temporal variation of the agreement between OA estimate and IMPROVE OA**

570   Besides August 2013 (see Fig. 6), the correlations between the OA estimate and

571   IMPROVE OA for the summer months June-July-August 2008-2013 were also examined

572   and shown in Fig. 7. Generally, the correlation coefficients between the OA estimate and

573   IMPROVE OA were >0.5 for summer months of the years investigated. The correlation

574   coefficients were generally higher in June compared to July and August. The lower

575   average temperature in June might be related to the higher correlation coefficients.

576   IMPROVE network aerosol samples were transported at ambient temperature in a truck

577   and more organic vapors likely evaporated at higher temperature. The different

578   temperatures and distances from IMPROVE sites to the laboratory may lead to

579   inhomogeneous evaporation among the samples and result in lower correlation

580   coefficients. Although higher temperatures in July and August may also lead to more BB,

581   average aerosol index over the US was not higher in July (mean: 0.35) and August

582   (mean: 0.36) compared to June (mean: 0.39) for these years. The underlying cause for the

583   lowest correlation coefficients in July and August 2012 is not clear and may be related

584   the severe drought in 2012 (Seco et al., 2015). The correlation coefficients were also low

585   for the linear regressions (not shown) of IMPROVE OA with both GEOS-Chem OA and

586   AOD-derived extinction. Because the lowest correlation coefficients were consistently

587   observed for multiple OA-related products and not just the OA estimate, we attributed

588   this to uncertainties in the IMPROVE OA measurements or some unknown bias shared

589   by the satellite HCHO, GEOS-Chem OA, and satellite AOD.

590
591

592   **6.7 South Korea OA estimate**

593   We attempted to estimate an OA estimate for South Korea, using airborne in situ

594   measurements of OA and HCHO from the KORUS-AQ field campaign (https://www-

595   air.larc.nasa.gov/missions/korus-aq/) and SAO OMI HCHO measurements. The National

596   Institute of Environmental Research (NIER) ground sites OC measurements during

597   KORUS-AQ over South Korea could be used to validate the OA estimate. However,

598   OMI HCHO measurements were below the detection limit (Zhu et al., 2016) in May

599   2016. Also, there were no OMI data available in June 2016 when airborne measurements

600   and ground sites OC measurements were available during KORUS-AQ. Because an OA

601   estimate for South Korea could not be well retrieved and validated, it was not presented

602   in this study.

603

604   **7   Limitations of the OA estimate and future work**

605   Because the OA estimate is based on satellite HCHO data, the detection limit of satellite

606   HCHO data affects the quality of the OA estimate. Currently, due to the limited

607   sensitivity of OMI for HCHO, the OA estimate is valid only when high levels of HCHO

608   are present, such as during summer time and near large HCHO sources. With the new

609   TROPOMI satellite instrument and future missions TEMPO and GEMS, satellite HCHO

Atmospheric
Chemistry
and Physics
Discussions

610   measurements will have higher spatial and temporal resolutions and lower detection

611   limits. These higher quality satellite HCHO measurements will improve our OA estimate

612   quality and also its spatial and temporal coverage.

613

614   Because the OA estimate uses the relationship of in situ HCHO and OA measurements,

615   the coverage of in situ aircraft field campaigns will impact the OA estimate quality.

616   Currently, in situ airborne measurements of OA and HCHO focus on the continental US.

617   Extending measurements to regions such as Africa BB, South America, and East Asia,

618   where HCHO and OA have high concentrations, will increase the spatial coverage of the

619   OA estimate product. Ground site measurements of OA with consistent quality control in

620   those regions will also be important for validating the OA estimate.

621

622   Improvement of satellite HCHO retrieval during the BB cases will also improve OA

623   estimate quality. BB cases with high UV aerosol index over the US were excluded in the

624   current OA estimate analysis. With improvement in the satellite retrieval of HCHO, we

625   may be able to estimate OA during BB cases over the US. Upcoming field campaigns

626   such as the Fire Influence on Regional and Global Environments Experiment – Air

627   Quality (FIREX-AQ) will provide opportunities to improve the analysis of OA estimate

628   in BB cases in the US.

629

630   This OA estimate method has limitations in remote regions far away from HCHO

631   sources. Because the lifetimes of HCHO (1-3 hours) and OA (1 week) are different, the

632   slopes and intercepts between HCHO and OA are expected to change when air masses

Atmospheric
Chemistry
and Physics
Discussions

633   are aged (e.g. in remote regions). OA vs. HCHO from SEAC^{4}RS and KORUS-AQ field

634   campaigns, color-coded with altitude, are plotted in Fig. S2 (a) and (b), respectively. A

635   relative depletion of HCHO at high altitudes was observed due to its shorter lifetime.

636   This also suggests that, at remote regions far away from the sources, the ratios of OA and

637   HCHO could be much higher and the relationship between OA and HCHO derived near

638   the sources may no longer apply. On the other hand, the lifetime of 1-3 hrs for HCHO

639   does not imply that the OA estimate only work within this timescale. HCHO is formed

640   from oxidation of transported gas phase VOCs, including the oxidation products of the

641   primary emitted VOCs, as well as of the slower reacting VOCs (e.g. Ethane and

642   Benzene). Most gas-to-particle oxidation processes that might produce HCHO can last up

643   to 1-2 days (Palm et al., 2018). Fig. S3 shows the ratios of OA and HCHO did not change

644   significantly downwind for the Rim Fire plume for about 1 day of aging, which was

645   determined by the distance from the source and the wind speed. A lower photolysis rate

646   of HCHO in the plume can also contribute to this. However, we do not expect that the

647   relationship of OA and HCHO remains past 1-2 boundary layer ventilation cycles (Palm

648   et al., 2018).

649

650

651   **8   Summary**

652   We have developed a satellite-based estimate of the surface OA concentration ("OA

653   estimate") based on in situ observations. This estimate is based on the empirical

654   relationships of in-situ OA and HCHO for several regions. OA and HCHO share VOC

655   sources with different yields and lifetimes. Using surface OA and HCHO linear

656   regression slopes and intercepts can relate surface HCHO to OA. To estimate the surface

657   HCHO concentration from satellite HCHO column, we used a vertical distribution factor

658   η, which is largely determined by boundary layer height and surface emissions and found

659   to reasonably retrieve surface HCHO from column HCHO.

660

661   The OA estimate over the continental US generally correlated well with EPA IMPROVE

662   network OA measurements corrected for partial evaporation. The good correlations are

663   not only for the time during SEAC[4]RS but also for most summer months over several

664   years (2008-2013) investigated. Compared to aerosol extinction derived from AOD, the

665   OA estimate had slightly higher correlation coefficients with IMPROVE OA. GEOS-

666   Chem can predict OA with a similar correlation coefficient with IMPROVE OA

667   compared to the OA estimate when GEOS-Chem was intensively validated with in situ

668   measurements for Southeast US. Better satellite HCHO data from TROPOMI and future

669   TEMPO and GEMS and extending spatiotemporal coverage of in situ measurements will

670   improve the quality and coverage of the OA estimate.

671

672

673

674

675

676

677

678

Atmospheric
Chemistry
and Physics
Discussions

691   References:

692   Anderson, D. C., Loughner, C. P., Diskin, G., Weinheimer, A., Canty, T. P., Salawitch, R. J.,
693   Worden, H. M., Fried, A., Mikoviny, T., Wisthaler, A., and Dickerson, R. R.: Measured and
694   modeled CO and NOy in DISCOVER-AQ: An evaluation of emissions and chemistry over the
695   eastern US, Atmos Environ, 96, 78-87, 10.1016/j.atmosenv.2014.07.004, 2014.
696
697   Attwood, A. R., Washenfelder, R. A., Brock, C. A., Hu, W., Baumann, K., Campuzano-Jost, P.,
698   Day, D. A., Edgerton, E. S., Murphy, D. M., Palm, B. B., McComiskey, A., Wagner, N. L., de
699   Sa, S. S., Ortega, A., Martin, S. T., Jimenez, J. L., and Brown, S. S.: Trends in sulfate and
700   organic aerosol mass in the Southeast U.S.: Impact on aerosol optical depth and radiative
701   forcing, Geophys Res Lett, 41, 7701-7709, 10.1002/2014gl061669, 2014.
702
703   Bahreini, R., Middlebrook, A. M., de Gouw, J. A., Warneke, C., Trainer, M., Brock, C. A., Stark,
704   H., Brown, S. S., Dube, W. P., Gilman, J. B., Hall, K., Holloway, J. S., Kuster, W. C., Perring,
705   A. E., Prevot, A. S. H., Schwarz, J. P., Spackman, J. R., Szidat, S., Wagner, N. L., Weber, R. J.,
706   Zotter, P., and Parrish, D. D.: Gasoline emissions dominate over diesel in formation of secondary
707   organic aerosol mass, Geophys Res Lett, 39, Artn L06805
708   10.1029/2011gl050718, 2012.
709
710   Baker, A. K., Beyersdorf, A. J., Doezema, L. A., Katzenstein, A., Meinardi, S., Simpson, I. J.,
711   Blake, D. R., and Rowland, F. S.: Measurements of nonmethane hydrocarbons in 28 United
712   States cities, Atmos Environ, 42, 170-182, 10.1016/j.atmosenv.2007.09.007, 2008.
713
714   Barth, M. C., Cantrell, C. A., Brune, W. H., Rutledge, S. A., Crawford, J. H., Huntrieser, H.,
715   Carey, L. D., MacGorman, D., Weisman, M., Pickering, K. E., Bruning, E., Anderson, B., Apel,
716   E., Biggerstaff, M., Campos, T., Campuzano-Jost, P., Cohen, R., Crounse, J., Day, D. A., Diskin,
717   G., Flocke, F., Fried, A., Garland, C., Heikes, B., Honomichl, S., Hornbrook, R., Huey, L. G.,
718   Jimenez, J. L., Lang, T., Lichtenstern, M., Mikoviny, T., Nault, B., O'Sullivan, D., Pan, L. L.,
719   Peischl, J., Pollack, I., Richter, D., Riemer, D., Ryerson, T., Schlager, H., St Clair, J., Walega, J.,
720   Weibring, P., Weinheimer, A., Wennberg, P., Wisthaler, A., Wooldridge, P. J., and Ziegler, C.:
721   The Deep Convective Clouds and Chemistry (Dc3) Field Campaign, B Am Meteorol Soc, 96,
722   1281-1309, 10.1175/Bams-D-13-00290.1, 2015.
723
724   Bianchi, F., Barmet, P., Stirnweis, L. El Haddad, I., Platt, S.M., Saurer, M., Lötscher, C.,
725   Siegwolf, R., Bigi, A., Hoyle, C.R., DeCarlo, P.F., Slowik, J.G., Prévôt, A.S.H., Baltensperger,
726   U., and Dommen. Contribution of methane to aerosol carbon mass. Atmospheric Environment,
727   141, 41-47, doi: 10.1016/j.atmosenv.2016.06.036, 2016.
728
729   Canagaratna, M. R., Jayne, J. T., Jimenez, J. L., Allan, J. D., Alfarra, M. R., Zhang, Q., Onasch,
730   T. B., Drewnick, F., Coe, H., Middlebrook, A., Delia, A., Williams, L. R., Trimborn, A. M.,
731   Northway, M. J., DeCarlo, P. F., Kolb, C. E., Davidovits, P., and Worsnop, D. R.: Chemical and
732   microphysical characterization of ambient aerosols with the aerodyne aerosol mass spectrometer,
733   Mass Spectrom Rev, 26, 185-222, 10.1002/mas.20115, 2007.
734
735   Carslaw, K. S., Lee, L. A., Reddington, C. L., Pringle, K. J., Rap, A., Forster, P. M., Mann, G.

Atmospheric
Chemistry
and Physics
Discussions

736   W., Spracklen, D. V., Woodhouse, M. T., Regayre, L. A., and Pierce, J. R.: Large contribution of
737   natural aerosols to uncertainty in indirect forcing, Nature, 503, 67-+, 10.1038/nature12674, 2013.
738

739   Cazorla, M., Wolfe, G. M., Bailey, S. A., Swanson, A. K., Arkinson, H. L., and Hanisco, T. F.: A
740   new airborne laser-induced fluorescence instrument for in situ detection of formaldehyde
741   throughout the troposphere and lower stratosphere, Atmos Meas Tech, 8, 541-552, 10.5194/amt-
742   8-541-2015, 2015.
743

744   Cubison, M. J., Ortega, A. M., Hayes, P. L., Farmer, D. K., Day, D., Lechner, M. J., Brune, W.
745   H., Apel, E., Diskin, G. S., Fisher, J. A., Fuelberg, H. E., Hecobian, A., Knapp, D. J., Mikoviny,
746   T., Riemer, D., Sachse, G. W., Sessions, W., Weber, R. J., Weinheimer, A. J., Wisthaler, A., and
747   Jimenez, J. L.: Effects of aging on organic aerosol from open biomass burning smoke in aircraft
748   and laboratory studies, Atmos. Chem. Phys., 11, 12049-12064, https://doi.org/10.5194/acp-11-
749   12049-2011, 2011.
750

751   Day, D. A., Wooldridge, P. J., Dillon, M. B., Thornton, J. A., and Cohen, R. C.: A thermal
752   dissociation laser-induced fluorescence instrument for in situ detection of NO2, peroxy nitrates,
753   alkyl nitrates, and HNO3, J Geophys Res-Atmos, 107, Artn 4046
754   10.1029/2001jd000779, 2002.
755

756   de Vries, M. J. M. P., Beirle, S., Hormann, C., Kaiser, J. W., Stammes, P., Tilstra, L. G.,
757   Tuinder, O. N. E., and Wagner, T.: A global aerosol classification algorithm incorporating
758   multiple satellite data sets of aerosol and trace gas abundances, Atmos Chem Phys, 15, 10597-
759   10618, 10.5194/acp-15-10597-2015, 2015.
760

761   DeCarlo, P. F., Kimmel, J. R., Trimborn, A., Northway, M. J., Jayne, J. T., Aiken, A. C., Gonin,
762   M., Fuhrer, K., Horvath, T., Docherty, K. S., Worsnop, D. R., and Jimenez, J. L.: Field-
763   deployable, high-resolution, time-of-flight aerosol mass spectrometer, Anal Chem, 78, 8281-
764   8289, 10.1021/ac061249n, 2006.
765

766   DeCarlo, P. F., Ulbrich, I. M., Crounse, J., de Foy, B., Dunlea, E. J., Aiken, A. C., Knapp, D.,
767   Weinheimer, A. J., Campos, T., Wennberg, P. O., and Jimenez, J. L.: Investigation of the sources
768   and processing of organic aerosol over the Central Mexican Plateau from aircraft measurements
769   during MILAGRO, Atmos. Chem. Phys., 10, 5257-5280, https://doi.org/10.5194/acp-10-5257-
770   2010, 2010.
771

772   DiGangi, J. P., Henry, S. B., Kammrath, A., Boyle, E. S., Kaser, L., Schnitzhofer, R., Graus, M.,
773   Turnipseed, A., Park, J. H., Weber, R. J., Hornbrook, R. S., Cantrell, C. A., Maudlin, R. L., Kim,
774   S., Nakashima, Y., Wolfe, G. M., Kajii, Y., Apel, E. C., Goldstein, A. H., Guenther, A., Karl, T.,
775   Hansel, A., and Keutsch, F. N.: Observations of glyoxal and formaldehyde as metrics for the
776   anthropogenic impact on rural photochemistry, Atmos Chem Phys, 12, 9529-9543, 10.5194/acp-
777   12-9529-2012, 2012.
778

779   Drewnick, F., Hings, S. S., DeCarlo, P., Jayne, J. T., Gonin, M., Fuhrer, K., Weimer, S.,
780   Jimenez, J. L., Demerjian, K. L., Borrmann, S., and Worsnop, D. R.: A new time-of-flight
781   aerosol mass spectrometer (TOF-AMS) - Instrument description and first field deployment,

Atmospheric
Chemistry
and Physics
Discussions

782   Aerosol Sci Tech, 39, 637-658, 10.1080/02786820500182040, 2005.
783

784   Dunlea, E. J., DeCarlo, P. F., Aiken, A. C., Kimmel, J. R., Peltier, R. E., Weber, R. J.,
785   Tomlinson, J., Collins, D. R., Shinozuka, Y., McNaughton, C. S., Howell, S. G., Clarke, A. D.,
786   Emmons, L. K., Apel, E. C., Pfister, G. G., van Donkelaar, A., Martin, R. V., Millet, D. B.,
787   Heald, C. L., and Jimenez, J. L.: Evolution of Asian aerosols during transpacific transport in
788   INTEX-B, Atmos Chem Phys, 9, 7257-7287, DOI 10.5194/acp-9-7257-2009, 2009.
789

790   Edgerton, E. S., Hartsell, B. E., Saylor, R. D., Jansen, J. J., Hansen, D. A., and Hidy, G. M.: The
791   Southeastern Aerosol Research and Characterization Study, part 3: Continuous measurements of
792   fine particulate matter mass and composition, J Air Waste Manage, 56, 1325-1341, Doi
793   10.1080/10473289.2006.10464585, 2006.
794

795   Forrister, H., Liu, J., Scheuer, E., Dibb, J., Ziemba, L., Thornhill, K. L., Anderson, B., Diskin,
796   G., Perring, A. E., Schwarz, J. P., Campuzano-Jost, P., Day, D. A., Palm, B. B., Jimenez, J. L.,
797   Nenes, A., and Weber, R. J.: Evolution of brown carbon in wildfire plumes, Geophys Res Lett,
798   42, 4623-4630, 10.1002/2015gl063897, 2015.
799

800   Gelaro, R., McCarty, W., Suarez, M. J., Todling, R., Molod, A., Takacs, L., Randles, C. A.,
801   Darmenov, A., Bosilovich, M. G., Reichle, R., Wargan, K., Coy, L., Cullather, R., Draper, C.,
802   Akella, S., Buchard, V., Conaty, A., da Silva, A. M., Gu, W., Kim, G. K., Koster, R., Lucchesi,
803   R., Merkova, D., Nielsen, J. E., Partyka, G., Pawson, S., Putman, W., Rienecker, M., Schubert,
804   S. D., Sienkiewicz, M., and Zhao, B.: The Modern-Era Retrospective Analysis for Research and
805   Applications, Version 2 (MERRA-2), J Climate, 30, 5419-5454, 10.1175/Jcli-D-16-0758.1,
806   2017.
807

808   Gonzalez Abad, G. G., Liu, X., Chance, K., Wang, H., Kurosu, T. P., and Suleiman, R.: Updated
809   Smithsonian Astrophysical Observatory Ozone Monitoring Instrument (SAO OMI)
810   formaldehyde retrieval, Atmos Meas Tech, 8, 19-32, 10.5194/amt-8-19-2015, 2015.
811

812   Guenther, A., Karl, T., Harley, P., Wiedinmyer, C., Palmer, P. I., and Geron, C.: Estimates of
813   global terrestrial isoprene emissions using MEGAN (Model of Emissions of Gases and Aerosols
814   from Nature), Atmos Chem Phys, 6, 3181-3210, DOI 10.5194/acp-6-3181-2006, 2006.
815

816   Hayes, P. L., Ortega, A. M., Cubison, M. J., Froyd, K. D., Zhao, Y., Cliff, S. S., Hu, W. W.,
817   Toohey, D. W., Flynn, J. H., Lefer, B. L., Grossberg, N., Alvarez, S., Rappenglueck, B., Taylor,
818   J. W., Allan, J. D., Holloway, J. S., Gilman, J. B., Kuster, W. C., De Gouw, J. A., Massoli, P.,
819   Zhang, X., Liu, J., Weber, R. J., Corrigan, A. L., Russell, L. M., Isaacman, G., Worton, D. R.,
820   Kreisberg, N. M., Goldstein, A. H., Thalman, R., Waxman, E. M., Volkamer, R., Lin, Y. H.,
821   Surratt, J. D., Kleindienst, T. E., Offenberg, J. H., Dusanter, S., Griffith, S., Stevens, P. S.,
822   Brioude, J., Angevine, W. M., and Jimenez, J. L.: Organic aerosol composition and sources in
823   Pasadena, California, during the 2010 CalNex campaign, J Geophys Res-Atmos, 118, 9233-
824   9257, 10.1002/jgrd.50530, 2013.
825

826   Hand, J. L., Schichtel, B. A., Malm, W. C., and Frank, N. H.: Spatial and Temporal Trends in
827   PM2.5 Organic and Elemental Carbon across the United States, Adv Meteorol, Artn 367674,

828   10.1155/2013/367674, 2013.
829
830   Hand, J. L., Schichtel, B. A., Malm, W. C., Pitchford, M., and Frank, N. H.: Spatial and seasonal
831   patterns in urban influence on regional concentrations of speciated aerosols across the United
832   States, J Geophys Res-Atmos, 119, 12832-12849, 10.1002/2014jd022328, 2014.
833
834   Hayes, P. L., Carlton, A. G., Baker, K. R., Ahmadov, R., Washenfelder, R. A., Alvarez, S.,
835   Rappenglück, B., Gilman, J. B., Kuster, W. C., de Gouw, J. A., Zotter, P., Prévôt, A. S. H.,
836   Szidat, S., Kleindienst, T. E., Offenberg, J. H., Ma, P. K., and Jimenez, J. L.: Modeling the
837   formation and aging of secondary organic aerosols in Los Angeles during CalNex 2010, Atmos.
838   Chem. Phys., 15, 5773-5801, https://doi.org/10.5194/acp-15-5773-2015, 2015.
839
840   Heald, C. L., Coe, H., Jimenez, J. L., Weber, R. J., Bahreini, R., Middlebrook, A. M., Russell, L.
841   M., Jolleys, M., Fu, T. M., Allan, J. D., Bower, K. N., Capes, G., Crosier, J., Morgan, W. T.,
842   Robinson, N. H., Williams, P. I., Cubison, M. J., DeCarlo, P. F., and Dunlea, E. J.: Exploring the
843   vertical profile of atmospheric organic aerosol: comparing 17 aircraft field campaigns with a
844   global model, Atmos Chem Phys, 11, 12673-12696, 10.5194/acp-11-12673-2011, 2011.
845
846   Heald, C. L., Goldstein, A. H., Allan, J. D., Aiken, A. C., Apel, E., Atlas, E. L., Baker, A. K.,
847   Bates, T. S., Beyersdorf, A. J., Blake, D. R., Campos, T., Coe, H., Crounse, J. D., DeCarlo, P. F.,
848   de Gouw, J. A., Dunlea, E. J., Flocke, F. M., Fried, A., Goldan, P., Griffin, R. J., Herndon, S. C.,
849   Holloway, J. S., Holzinger, R., Jimenez, J. L., Junkermann, W., Kuster, W. C., Lewis, A. C.,
850   Meinardi, S., Millet, D. B., Onasch, T., Polidori, A., Quinn, P. K., Riemer, D. D., Roberts, J. M.,
851   Salcedo, D., Sive, B., Swanson, A. L., Talbot, R., Warneke, C., Weber, R. J., Weibring, P.,
852   Wennberg, P. O., Worsnop, D. R., Wittig, A. E., Zhang, R., Zheng, J., and Zheng, W.: Total
853   observed organic carbon (TOOC) in the atmosphere: a synthesis of North American
854   observations, Atmos Chem Phys, 8, 2007-2025, 10.5194/acp-8-2007-2008, 2008.
855
856   Hidy, G. M., Blanchard, C. L., Baumann, K., Edgerton, E., Tanenbaum, S., Shaw, S., Knipping,
857   E., Tombach, I., Jansen, J., and Walters, J.: Chemical climatology of the southeastern United
858   States, 1999-2013, Atmos Chem Phys, 14, 11893-11914, 10.5194/acp-14-11893-2014, 2014.
859
860   Hodzic, A., and Jimenez, J. L.: Modeling anthropogenically controlled secondary organic
861   aerosols in a megacity: a simplified framework for global and climate models, Geosci Model
862   Dev, 4, 901-917, 10.5194/gmd-4-901-2011, 2011.
863
864   Hu, W. W., Campuzano-Jost, P., Palm, B. B., Day, D. A., Ortega, A. M., Hayes, P. L.,
865   Krechmer, J. E., Chen, Q., Kuwata, M., Liu, Y. J., de Sá, S. S., McKinney, K., Martin, S. T., Hu,
866   M., Budisulistiorini, S. H., Riva, M., Surratt, J. D., St. Clair, J. M., Isaacman-Van Wertz, G.,
867   Yee, L. D., Goldstein, A. H., Carbone, S., Brito, J., Artaxo, P., de Gouw, J. A., Koss, A.,
868   Wisthaler, A., Mikoviny, T., Karl, T., Kaser, L., Jud, W., Hansel, A., Docherty, K. S., Alexander,
869   M. L., Robinson, N. H., Coe, H., Allan, J. D., Canagaratna, M. R., Paulot, F., and Jimenez, J. L.:
870   Characterization of a real-time tracer for isoprene epoxydiols-derived secondary organic aerosol
871   (IEPOX-SOA) from aerosol mass spectrometer measurements, Atmos. Chem. Phys., 15, 11807-
872   11833, https://doi.org/10.5194/acp-15-11807-2015, 2015.
873

874   Hudson, P. K., Murphy, D. M., Cziczo, D. J., Thomson, D. S., de Gouw, J. A., Warneke, C.,
875   Holloway, J., Jost, J. R., and Hubler, G.: Biomass-burning particle measurements: Characteristic
876   composition and chemical processing, J Geophys Res-Atmos, 109, Artn D23s27
877   10.1029/2003jd004398, 2004.
878
879   Jimenez, J. L., Canagaratna, M. R., Donahue, N. M., Prevot, A. S. H., Zhang, Q., Kroll, J. H.,
880   DeCarlo, P. F., Allan, J. D., Coe, H., Ng, N. L., Aiken, A. C., Docherty, K. S., Ulbrich, I. M.,
881   Grieshop, A. P., Robinson, A. L., Duplissy, J., Smith, J. D., Wilson, K. R., Lanz, V. A., Hueglin,
882   C., Sun, Y. L., Tian, J., Laaksonen, A., Raatikainen, T., Rautiainen, J., Vaattovaara, P., Ehn, M.,
883   Kulmala, M., Tomlinson, J. M., Collins, D. R., Cubison, M. J., Dunlea, E. J., Huffman, J. A.,
884   Onasch, T. B., Alfarra, M. R., Williams, P. I., Bower, K., Kondo, Y., Schneider, J., Drewnick, F.,
885   Borrmann, S., Weimer, S., Demerjian, K., Salcedo, D., Cottrell, L., Griffin, R., Takami, A.,
886   Miyoshi, T., Hatakeyama, S., Shimono, A., Sun, J. Y., Zhang, Y. M., Dzepina, K., Kimmel, J.
887   R., Sueper, D., Jayne, J. T., Herndon, S. C., Trimborn, A. M., Williams, L. R., Wood, E. C.,
888   Middlebrook, A. M., Kolb, C. E., Baltensperger, U., and Worsnop, D. R.: Evolution of Organic
889   Aerosols in the Atmosphere, Science, 326, 1525-1529, 10.1126/science.1180353, 2009.
890   Jimenez, J. L., Canagaratna, M. R., Drewnick, F., Allan, J. D., Alfarra, M. R., Middlebrook, A.
891   M., Slowik, J. G., Zhang, Q., Coe, H., Jayne, J. T., and Worsnop, D. R.: Comment on "The
892   effects of molecular weight and thermal decomposition on the sensitivity of a thermal desorption
893   aerosol mass spectrometer", Aerosol Sci Tech, 50, I-Xv, 10.1080/02786826.2016.1205728,
894   2016.
895
896   Kahn, R. A., and Gaitley, B. J.: An analysis of global aerosol type as retrieved by MISR, J
897   Geophys Res-Atmos, 120, 4248-4281, 10.1002/2015jd023322, 2015.
898
899   Kaiser, J., Jacob, D. J., Zhu, L., Travis, K. R., Fisher, J. A., Abad, G. G., Zhang, L., Zhang, X.
900   S., Fried, A., Crounse, J. D., St Clair, J. M., and Wisthaler, A.: High-resolution inversion of OMI
901   formaldehyde columns to quantify isoprene emission on ecosystem-relevant scales: application
902   to the southeast US, Atmos Chem Phys, 18, 5483-5497, 10.5194/acp-18-5483-2018, 2018.
903
904   Kiehl, J. T., and Briegleb, B. P.: The Relative Roles of Sulfate Aerosols and Greenhouse Gases
905   in Climate Forcing, Science, 260, 311-314, DOI 10.1126/science.260.5106.311, 1993.
906
907   Kim, P. S., Jacob, D. J., Fisher, J. A., Travis, K., Yu, K., Zhu, L., Yantosca, R. M., Sulprizio, M.
908   P., Jimenez, J. L., Campuzano-Jost, P., Froyd, K. D., Liao, J., Hair, J. W., Fenn, M. A., Butler, C.
909   F., Wagner, N. L., Gordon, T. D., Welti, A., Wennberg, P. O., Crounse, J. D., St Clair, J. M.,
910   Teng, A. P., Millet, D. B., Schwarz, J. P., Markovic, M. Z., and Perring, A. E.: Sources,
911   seasonality, and trends of southeast US aerosol: an integrated analysis of surface, aircraft, and
912   satellite observations with the GEOS-Chem chemical transport model, Atmos Chem Phys, 15,
913   10411-10433, 10.5194/acp-15-10411-2015, 2015.
914
915   Kroll, J. H., Ng, N. L., Murphy, S. M., Flagan, R. C., and Seinfeld, J. H.: Secondary organic
916   aerosol formation from isoprene photooxidation, Environ Sci Technol, 40, 1869-1877,
917   10.1021/es0524301, 2006.
918
919   Lamarque, J. F., Bond, T. C., Eyring, V., Granier, C., Heil, A., Klimont, Z., Lee, D., Liousse, C.,

Atmospheric
Chemistry
and Physics
Discussions

920 Mieville, A., Owen, B., Schultz, M. G., Shindell, D., Smith, S. J., Stehfest, E., Van Aardenne, J.,
921 Cooper, O. R., Kainuma, M., Mahowald, N., McConnell, J. R., Naik, V., Riahi, K., and van
922 Vuuren, D. P.: Historical (1850-2000) gridded anthropogenic and biomass burning emissions of
923 reactive gases and aerosols: methodology and application, Atmos Chem Phys, 10, 7017-7039,
924 10.5194/acp-10-7017-2010, 2010.
925
926 Lamsal, L. N., Krotkov, N. A., Celarier, E. A., Swartz, W. H., Pickering, K. E., Bucsela, E. J.,
927 Gleason, J. F., Martin, R. V., Philip, S., Irie, H., Cede, A., Herman, J., Weinheimer, A.,
928 Szykman, J. J., and Knepp, T. N.: Evaluation of OMI operational standard NO2 column
929 retrievals using in situ and surface-based NO2 observations, Atmos Chem Phys, 14, 11587-
930 11609, 10.5194/acp-14-11587-2014, 2014.
931
932 Lee-Taylor, J., Hodzic, A., Madronich, S., Aumont, B., Camredon, M., and Valorso, R.:
933 Multiday production of condensing organic aerosol mass in urban and forest outflow, Atmos
934 Chem Phys, 15, 595-615, 10.5194/acp-15-595-2015, 2015.
935
936 Levelt, P. F., Van den Oord, G. H. J., Dobber, M. R., Malkki, A., Visser, H., de Vries, J.,
937 Stammes, P., Lundell, J. O. V., and Saari, H.: The Ozone Monitoring Instrument, Ieee T Geosci
938 Remote, 44, 1093-1101, 10.1109/Tgrs.2006.872333, 2006.
939
940 Levy, R. C., Munchak, L. A., Mattoo, S., Patadia, F., Remer, L. A., and Holz, R. E.: Towards a
941 long-term global aerosol optical depth record: applying a consistent aerosol retrieval algorithm to
942 MODIS and VIIRS-observed reflectance, Atmos Meas Tech, 8, 4083-4110, 10.5194/amt-8-
943 4083-2015, 2015.
944
945 Liu, X. X., Huey, L. G., Yokelson, R. J., Selimovic, V., Simpson, I. J., Muller, M., Jimenez, J.
946 L., Campuzano-Jost, P., Beyersdorf, A. J., Blake, D. R., Butterfield, Z., Choi, Y., Crounse, J. D.,
947 Day, D. A., Diskin, G. S., Dubey, M. K., Fortner, E., Hanisco, T. F., Hu, W. W., King, L. E.,
948 Kleinman, L., Meinardi, S., Mikoviny, T., Onasch, T. B., Palm, B. B., Peischl, J., Pollack, I. B.,
949 Ryerson, T. B., Sachse, G. W., Sedlacek, A. J., Shilling, J. E., Springston, S., St Clair, J. M.,
950 Tanner, D. J., Teng, A. P., Wennberg, P. O., Wisthaler, A., and Wolfe, G. M.: Airborne
951 measurements of western US wildfire emissions: Comparison with prescribed burning and air
952 quality implications, J Geophys Res-Atmos, 122, 6108-6129, 10.1002/2016jd026315, 2017.
953 Malm, W. C., Sisler, J. F., Huffman, D., Eldred, R. A., and Cahill, T. A.: Spatial and Seasonal
954 Trends in Particle Concentration and Optical Extinction in the United-States, J Geophys Res-
955 Atmos, 99, 1347-1370, Doi 10.1029/93jd02916, 1994.
956
957 Malm, W. C., Schichtel, B. A., Hand, J. L., and Collett, J. L.: Concurrent Temporal and Spatial
958 Trends in Sulfate and Organic Mass Concentrations Measured in the IMPROVE Monitoring
959 Program, J Geophys Res-Atmos, 122, 10341-10355, 10.1002/2017jd026865, 2017.
960
961 Marais, E. A., Jacob, D. J., Jimenez, J. L., Campuzano-Jost, P., Day, D. A., Hu, W., Krechmer,
962 J., Zhu, L., Kim, P. S., Miller, C. C., Fisher, J. A., Travis, K., Yu, K., Hanisco, T. F., Wolfe, G.
963 M., Arkinson, H. L., Pye, H. O. T., Froyd, K. D., Liao, J., and McNeill, V. F.: Aqueous-phase
964 mechanism for secondary organic aerosol formation from isoprene: application to the southeast
965 United States and co-benefit of SO2 emission controls, Atmos Chem Phys, 16, 1603-1618,

Atmospheric
Chemistry
and Physics
Discussions

966   10.5194/acp-16-1603-2016, 2016.
967
968   Marais, E. A., Jacob, D. J., Turner, J. R., and Mickley, L. J.: Evidence of 1991-2013 decrease of
969   biogenic secondary organic aerosol in response to SO2 emission controls, Environ Res Lett, 12,
970   ARTN 054018
971   10.1088/1748-9326/aa69c8, 2017.
972
973   McDonald, B. C., de Gouw, J. A., Gilman, J. B., Jathar, S. H., Akherati, A., Cappa, C. D.,
974   Jimenez, J. L., Lee-Taylor, J., Hayes, P. L., McKeen, S. A., Cui, Y. Y., Kim, S. W., Gentner, D.
975   R., Isaacman-VanWertz, G., Goldstein, A. H., Harley, R. A., Frost, G. J., Roberts, J. M.,
976   Ryerson, T. B., and Trainer, M.: Volatile chemical products emerging as largest petrochemical
977   source of urban organic emissions, Science, 359, 760-764, ARTN aaq0524
978   10.1126/science.aaq0524, 2018.
979
980   Millet, D. B., Jacob, D. J., Boersma, K. F., Fu, T. M., Kurosu, T. P., Chance, K., Heald, C. L.,
981   and Guenther, A.: Spatial distribution of isoprene emissions from North America derived from
982   formaldehyde column measurements by the OMI satellite sensor, J Geophys Res-Atmos, 113,
983   Artn D02307
984   10.1029/2007jd008950, 2008.
985
986   Murphy, D. M., Cziczo, D. J., Froyd, K. D., Hudson, P. K., Matthew, B. M., Middlebrook, A.
987   M., Peltier, R. E., Sullivan, A., Thomson, D. S., and Weber, R. J.: Single-particle mass
988   spectrometry of tropospheric aerosol particles, J Geophys Res-Atmos, 111, Artn D23s32
989   10.1029/2006jd007340, 2006.
990
991   Na, K., Kim, Y. P., and Moon, K. C.: Seasonal variation of the C-2-C-9 hydrocarbons
992   concentrations and compositions emitted from motor vehicles in a Seoul tunnel, Atmos Environ,
993   36, 1969-1978, Pii S1352-2310(02)00149-8
994   Doi 10.1016/S1352-2310(02)00149-8, 2002.
995
996   Na, K., Moon, K. C., and Kim, Y. P.: Source contribution to aromatic VOC concentration and
997   ozone formation potential in the atmosphere of Seoul, Atmos Environ, 39, 5517-5524,
998   10.1016/j.atmosenv.2005.06.005, 2005.
999
1000   B. A. Nault, P. Campuzano-Jost, D. A. Day, J. C. Schroder, D. R. Blake, M. R. Canagaratna, J.
1001   A. de Gouw, F. Flocke, A. Fried, J. B. Gilman, T. F. Hanisco, L. G. Huey, B. T. Jobson, W. C.
1002   Kuster, B. Lefer, J. Liao, D. D. Montzka, I. B. Pollack, J. Peischl, B. Rappenglueck, J. M.
1003   Roberts, T. B. Ryerson, J.Stutz, P. Weibring, A. J. Weinheimer, E. C. Wood, and J. L. Jimenez:
1004   Quantification of the Rapid Photochemical Secondary Organic Aerosol Production Observed
1005   across Megacities around the World, in preparation for submission to Nature Geoscience or
1006   PNAS.
1007
1008   Ng, N. L., Kroll, J. H., Chan, A. W. H., Chhabra, P. S., Flagan, R. C., and Seinfeld, J. H.:
1009   Secondary organic aerosol formation from m-xylene, toluene, and benzene, Atmos Chem Phys,
1010   7, 3909-3922, DOI 10.5194/acp-7-3909-2007, 2007.
1011

Ovadnevaite, J., Zuend, A., Laaksonen, A., Sanchez, K. J., Roberts, G., Ceburnis, D., Decesari, S., Rinaldi, M., Hodas, N., Facchini, M. C., Seinfeld, J. H., and Dowd, C. O.: Surface tension prevails over solute effect in organic-influenced cloud droplet activation, Nature, 546, 637-641, 10.1038/nature22806, 2017.

Palm, B. B., de Sa, S. S., Day, D. A., Campuzano-Jost, P., Hu, W. W., Seco, R., Sjostedt, S. J., Park, J. H., Guenther, A. B., Kim, S., Brito, J., Wurm, F., Artaxo, P., Thalman, R., Wang, J., Yee, L. D., Wernis, R., Isaacman-VanWertz, G., Goldstein, A. H., Liu, Y. J., Springston, S. R., Souza, R., Newburn, M. K., Alexander, M. L., Martin, S. T., and Jimenez, J. L.: Secondary organic aerosol formation from ambient air in an oxidation flow reactor in central Amazonia, Atmos Chem Phys, 18, 467-493, 10.5194/acp-18-467-2018, 2018.

Pope, C. A., Burnett, R. T., Thun, M. J., Calle, E. E., Krewski, D., Ito, K., and Thurston, G. D.: Lung cancer, cardiopulmonary mortality, and long-term exposure to fine particulate air pollution, Jama-J Am Med Assoc, 287, 1132-1141, DOI 10.1001/jama.287.9.1132, 2002.

Pye, H. O. T., Chan, A. W. H., Barkley, M. P., and Seinfeld, J. H.: Global modeling of organic aerosol: the importance of reactive nitrogen (NOx and NO3), Atmos Chem Phys, 10, 11261-11276, 10.5194/acp-10-11261-2010, 2010.

Pye, H. O. T., Murphy, B. N., Xu, L., Ng, N. L., Carlton, A. G., Guo, H., Weber, R., Vasilakos, P., Appel, K. W., Budisulistiorini, S. H., Surratt, J. D., Nenes, A., Hu, W., Jimenez, J. L., Isaacman-VanWertz, G., Misztal, P. K., and Goldstein, A. H.: On the implications of aerosol liquid water and phase separation for organic aerosol mass, Atmos. Chem. Phys., 17, 343-369, https://doi.org/10.5194/acp-17-343-2017, 2017.

Richter, D., Weibring, P., Walega, J. G., Fried, A., Spuler, S. M., and Taubman, M. S.: Compact highly sensitive multi-species airborne mid-IR spectrometer, Appl Phys B-Lasers O, 119, 119-131, 10.1007/s00340-015-6038-8, 2015.

Ridley, D. A., Heald, C. L., Ridley, K. J., and Kroll, J. H.: Causes and consequences of decreasing atmospheric organic aerosol in the United States, P Natl Acad Sci USA, 115, 290-295, 10.1073/pnas.1700387115, 2018.

Robinson, A. L., Donahue, N. M., Shrivastava, M. K., Weitkamp, E. A., Sage, A. M., Grieshop, A. P., Lane, T. E., Pierce, J. R., and Pandis, S. N.: Rethinking organic aerosols: Semivolatile emissions and photochemical aging, Science, 315, 1259-1262, 10.1126/science.1133061, 2007.
Ryerson, T. B., Andrews, A. E., Angevine, W. M., Bates, T. S., Brock, C. A., Cairns, B., Cohen, R. C., Cooper, O. R., de Gouw, J. A., Fehsenfeld, F. C., Ferrare, R. A., Fischer, M. L., Flagan, R. C., Goldstein, A. H., Hair, J. W., Hardesty, R. M., Hostetler, C. A., Jimenez, J. L., Langford, A. O., McCauley, E., McKeen, S. A., Molina, L. T., Nenes, A., Oltmans, S. J., Parrish, D. D., Pederson, J. R., Pierce, R. B., Prather, K., Quinn, P. K., Seinfeld, J. H., Senff, C. J., Sorooshian, A., Stutz, J., Surratt, J. D., Trainer, M., Volkamer, R., Williams, E. J., and Wofsy, S. C.: The 2010 California Research at the Nexus of Air Quality and Climate Change (CalNex) field study, J Geophys Res-Atmos, 118, 5830-5866, 10.1002/jgrd.50331, 2013.

Atmospheric
Chemistry
and Physics
Discussions

Open Access

EGU

1058 Ryerson, T. B., Trainer, M., Holloway, J. S., Parrish, D. D., Huey, L. G., Sueper, D. T., Frost, G.
1059 J., Donnelly, S. G., Schauffler, S., Atlas, E. L., Kuster, W. C., Goldan, P. D., Hubler, G.,
1060 Meagher, J. F., and Fehsenfeld, F. C.: Observations of ozone formation in power plant plumes
1061 and implications for ozone control strategies, Science, 292, 719-723, DOI
1062 10.1126/science.1058113, 2001.
1063
1064 Seco, R., Karl, T., Guenther, A., Hosman, K. P., Pallardy, S. G., Gu, L. H., Geron, C., Harley, P.,
1065 and Kim, S.: Ecosystem-scale volatile organic compound fluxes during an extreme drought in a
1066 broadleaf temperate forest of the Missouri Ozarks (central USA), Global Change Biol, 21, 3657-
1067 3674, 10.1111/gcb.12980, 2015.
1068
1069 Schroder, J.C, P. Campuzano-Jost, D.A. Day, V. Shah, K. Larson, J.M. Sommers, A.P. Sullivan,
1070 T. Campos, J.M. Reeves, A. Hills, R. S. Hornbrook, N.J. Blake, E. Scheuer, H. Guo, D.L.
1071 Fibiger, E.E. McDuffie, P.L. Hayes, R.J. Weber, J.E. Dibb, E.C. Apel, L. Jaeglé, S.S. Brown,
1072 J.A. Thornton, J.L. Jimenez. Sources and Secondary Production of Organic Aerosols in the
1073 Northeastern US during WINTER. J. Geophys. Res.-Atmos., revised, 2018.
1074
1075 Shrivastava, M., Cappa, C. D., Fan, J. W., Goldstein, A. H., Guenther, A. B., Jimenez, J. L.,
1076 Kuang, C., Laskin, A., Martin, S. T., Ng, N. L., Petaja, T., Pierce, J. R., Rasch, P. J., Roldin, P.,
1077 Seinfeld, J. H., Shilling, J., Smith, J. N., Thornton, J. A., Volkamer, R., Wang, J., Worsnop, D.
1078 R., Zaveri, R. A., Zelenyuk, A., and Zhang, Q.: Recent advances in understanding secondary
1079 organic aerosol: Implications for global climate forcing, Rev Geophys, 55, 509-559,
1080 10.1002/2016rg000540, 2017.
1081
1082 Solomon, P. A., Crumpler, D., Flanagan, J. B., Jayanty, R. K. M., Rickman, E. E., and McDade,
1083 C. E.: US National PM2.5 Chemical Speciation Monitoring Networks-CSN and IMPROVE:
1084 Description of networks, J Air Waste Manage, 64, 1410-1438, 10.1080/10962247.2014.956904,
1085 2014.
1086
1087 Stocker, T.F., D. Qin, G.-K. Plattner, M. Tignor, S.K. Allen, J. Boschung, A. Nauels, Y.
1088 Xia, V. Bex and P.M. Midgley (eds.), IPCC, 2013: *Climate Change 2013: The Physical*
1089 *Science Basis. Contribution of Working Group I to the Fifth Assessment Report of the*
1090 *Intergovernmental Panel on Climate Change.* Cambridge University Press, Cambridge,
1091 United Kingdom and New York, NY, USA, 1535 pp, doi:10.1017/CBO9781107415324.
1092
1093
1094 Taylor, K. E., and Penner, J. E.: Response of the Climate System to Atmospheric Aerosols and
1095 Greenhouse Gases, Nature, 369, 734-737, DOI 10.1038/369734a0, 1994.
1096
1097 Tong, D. Q., Lamsal, L., Pan, L., Ding, C., Kim, H., Lee, P., Chai, T. F., Pickering, K. E., and
1098 Stajner, I.: Long-term NOx trends over large cities in the United States during the great
1099 recession: Comparison of satellite retrievals, ground observations, and emission inventories,
1100 Atmos Environ, 107, 70-84, 10.1016/j.atmosenv.2015.01.035, 2015.
1101
1102 Toon, O. B., Maring, H., Dibb, J., Ferrare, R., Jacob, D. J., Jensen, E. J., Luo, Z. J., Mace, G. G.,
1103 Pan, L. L., Pfister, L., Rosenlof, K. H., Redemann, J., Reid, J. S., Singh, H. B., Thompson, A.

1104   M., Yokelson, R., Minnis, P., Chen, G., Jucks, K. W., and Pszenny, A.: Planning,
1105   implementation, and scientific goals of the Studies of Emissions and Atmospheric Composition,
1106   Clouds and Climate Coupling by Regional Surveys (SEAC(4)RS) field mission, J Geophys Res-
1107   Atmos, 121, 4967-5009, 10.1002/2015jd024297, 2016.
1108
1109   Torres, O., Tanskanen, A., Veihelmann, B., Ahn, C., Braak, R., Bhartia, P. K., Veefkind, P., and
1110   Levelt, P.: Aerosols and surface UV products from Ozone Monitoring Instrument observations:
1111   An overview, J Geophys Res-Atmos, 112, Artn D24s47
1112   10.1029/2007jd008809, 2007.
1113
1114   Travis, K. R., Jacob, D. J., Fisher, J. A., Kim, P. S., Marais, E. A., Zhu, L., Yu, K., Miller, C. C.,
1115   Yantosca, R. M., Sulprizio, M. P., Thompson, A. M., Wennberg, P. O., Crounse, J. D., St Clair,
1116   J. M., Cohen, R. C., Laughner, J. L., Dibb, J. E., Hall, S. R., Ullmann, K., Wolfe, G. M., Pollack,
1117   I. B., Peischl, J., Neuman, J. A., and Zhou, X. L.: Why do models overestimate surface ozone in
1118   the Southeast United States?, Atmos Chem Phys, 16, 13561-13577, 10.5194/acp-16-13561-2016,
1119   2016.
1120
1121   Tsigaridis, K., Daskalakis, N., Kanakidou, M., Adams, P. J., Artaxo, P., Bahadur, R., Balkanski,
1122   Y., Bauer, S. E., Bellouin, N., Benedetti, A., Bergman, T., Berntsen, T. K., Beukes, J. P., Bian,
1123   H., Carslaw, K. S., Chin, M., Curci, G., Diehl, T., Easter, R. C., Ghan, S. J., Gong, S. L., Hodzic,
1124   A., Hoyle, C. R., Iversen, T., Jathar, S., Jimenez, J. L., Kaiser, J. W., Kirkevag, A., Koch, D.,
1125   Kokkola, H., Lee, Y. H., Lin, G., Liu, X., Luo, G., Ma, X., Mann, G. W., Mihalopoulos, N.,
1126   Morcrette, J. J., Muller, J. F., Myhre, G., Myriokefalitakis, S., Ng, N. L., O'Donnell, D., Penner,
1127   J. E., Pozzoli, L., Pringle, K. J., Russell, L. M., Schulz, M., Sciare, J., Seland, O., Shindell, D. T.,
1128   Sillman, S., Skeie, R. B., Spracklen, D., Stavrakou, T., Steenrod, S. D., Takemura, T., Tiitta, P.,
1129   Tilmes, S., Tost, H., van Noije, T., van Zyl, P. G., von Salzen, K., Yu, F., Wang, Z., Wang, Z.,
1130   Zaveri, R. A., Zhang, H., Zhang, K., Zhang, Q., and Zhang, X.: The AeroCom evaluation and
1131   intercomparison of organic aerosol in global models, Atmos Chem Phys, 14, 10845-10895,
1132   10.5194/acp-14-10845-2014, 2014.
1133
1134   Veefkind, J. P., Boersma, K. F., Wang, J., Kurosu, T. P., Krotkov, N., Chance, K., and Levelt, P.
1135   F.: Global satellite analysis of the relation between aerosols and short-lived trace gases, Atmos
1136   Chem Phys, 11, 1255-1267, 10.5194/acp-11-1255-2011, 2011.
1137
1138   Wagner, N. L., Brock, C. A., Angevine, W. M., Beyersdorf, A., Campuzano-Jost, P., Day, D., de
1139   Gouw, J. A., Diskin, G. S., Gordon, T. D., Graus, M. G., Holloway, J. S., Huey, G., Jimenez, J.
1140   L., Lack, D. A., Liao, J., Liu, X., Markovic, M. Z., Middlebrook, A. M., Mikoviny, T., Peischl,
1141   J., Perring, A. E., Richardson, M. S., Ryerson, T. B., Schwarz, J. P., Warneke, C., Welti, A.,
1142   Wisthaler, A., Ziemba, L. D., and Murphy, D. M.: In situ vertical profiles of aerosol extinction,
1143   mass, and composition over the southeast United States during SENEX and SEAC(4)RS:
1144   observations of a modest aerosol enhancement aloft, Atmos Chem Phys, 15, 7085-7102,
1145   10.5194/acp-15-7085-2015, 2015.
1146
1147   Walgraeve, C., Demeestere, K., Dewulf, J., Zimmermann, R., and Van Langenhove, H.:
1148   Oxygenated polycyclic aromatic hydrocarbons in atmospheric particulate matter: Molecular
1149   characterization and occurrence, Atmos Environ, 44, 1831-1846,

Atmospheric
Chemistry
and Physics
Discussions

1150   10.1016/j.atmosenv.2009.12.004, 2010.
1151

1152   Warneke, C., de Gouw, J. A., Stohl, A., Cooper, O. R., Goldan, P. D., Kuster, W. C., Holloway,
1153   J. S., Williams, E. J., Lerner, B. M., McKeen, S. A., Trainer, M., Fehsenfeld, F. C., Atlas, E. L.,
1154   Donnelly, S. G., Stroud, V., Lueb, A., and Kato, S.: Biomass burning and anthropogenic sources
1155   of CO over New England in the summer 2004, J Geophys Res-Atmos, 111, Artn D23s15
1156   10.1029/2005jd006878, 2006.
1157

1158   Warneke, C., Veres, P., Holloway, J. S., Stutz, J., Tsai, C., Alvarez, S., Rappenglueck, B.,
1159   Fehsenfeld, F. C., Graus, M., Gilman, J. B., and de Gouw, J. A.: Airborne formaldehyde
1160   measurements using PTR-MS: calibration, humidity dependence, inter-comparison and initial
1161   results, Atmos Meas Tech, 4, 2345-2358, 10.5194/amt-4-2345-2011, 2011.
1162

1163   Weibring, P., Richter, D., Fried, A., Walega, J. G., and Dyroff, C.: Ultra-high-precision mid-IR
1164   spectrometer II: system description and spectroscopic performance, Appl Phys B-Lasers O, 85,
1165   207-218, 10.1007/s00340-006-2300-4, 2006.
1166

1167   Wolfe, G. M., Kaiser, J., Hanisco, T. F., Keutsch, F. N., de Gouw, J. A., Gilman, J. B., Graus,
1168   M., Hatch, C. D., Holloway, J., Horowitz, L. W., Lee, B. H., Lerner, B. M., Lopez-Hilifiker, F.,
1169   Mao, J., Marvin, M. R., Peischl, J., Pollack, I. B., Roberts, J. M., Ryerson, T. B., Thornton, J. A.,
1170   Veres, P. R., and Warneke, C.: Formaldehyde production from isoprene oxidation across NOx
1171   regimes, Atmos Chem Phys, 16, 2597-2610, 10.5194/acp-16-2597-2016, 2016.
1172

1173   Worton, D.R., J.D. Surratt, B.W. Lafranchi, A.W.H. Chan, Y. Zhao, R. Weber, J. Park, J.B.
1174   Gilman, J. de Gouw, C. Park, G. Schade, M. Beaver, J. StClair, J. Crounse, P. Wennberg, G.
1175   Wolfe, S. Harrold, J. Thornton, D. K. Farmer, K.S. Docherty, Mi.J. Cubison, J.L. Jimenez, A.
1176   Frossard, L. Russell, K. Kristensen, M. Glasius, J. Mao, X. Ren, W.H. Brune, E. Browne, S.
1177   Pusede, R. Cohen, J.H. Seinfeld and A.H. Goldstein. Observational Insights into Aerosol
1178   Formation from Isoprene. Environmental Science & Technology, 47, 11403-11413,
1179   doi:10.1021/es4011064, 2013.
1180

1181   Xu, L., Middlebrook, A. M., Liao, J., de Gouw, J. A., Guo, H. Y., Weber, R. J., Nenes, A.,
1182   Lopez-Hilfiker, F. D., Lee, B. H., Thornton, J. A., Brock, C. A., Neuman, J. A., Nowak, J. B.,
1183   Pollack, I. B., Welti, A., Graus, M., Warneke, C., and Ng, N. L.: Enhanced formation of
1184   isoprene-derived organic aerosol in sulfur-rich power plant plumes during Southeast Nexus, J
1185   Geophys Res-Atmos, 121, 11137-11153, 10.1002/2016jd025156, 2016.
1186

1187   Xu, L., Suresh, S., Guo, H., Weber, R. J., and Ng, N. L.: Aerosol characterization over the
1188   southeastern United States using high-resolution aerosol mass spectrometry: spatial and seasonal
1189   variation of aerosol composition and sources with a focus on organic nitrates, Atmos Chem Phys,
1190   15, 7307-7336, 10.5194/acp-15-7307-2015, 2015.
1191

1192   Yu, K. R., Jacob, D. J., Fisher, J. A., Kim, P. S., Marais, E. A., Miller, C. C., Travis, K. R., Zhu,
1193   L., Yantosca, R. M., Sulprizio, M. P., Cohen, R. C., Dibb, J. E., Fried, A., Mikoviny, T.,
1194   Ryerson, T. B., Wennberg, P. O., and Wisthaler, A.: Sensitivity to grid resolution in the ability of
1195   a chemical transport model to simulate observed oxidant chemistry under high-isoprene

Atmospheric
Chemistry
and Physics
Discussions

1196   conditions, Atmos Chem Phys, 16, 4369-4378, 10.5194/acp-16-4369-2016, 2016.
1197

1198   Zhang, H. F., Yee, L. D., Lee, B. H., Curtis, M. P., Worton, D. R., Isaacman-VanWertz, G.,
1199   Offenberg, J. H., Lewandowski, M., Kleindienst, T. E., Beaver, M. R., Holder, A. L., Lonneman,
1200   W. A., Docherty, K. S., Jaoui, M., Pye, H. O. T., Hu, W. W., Day, D. A., Campuzano-Jost, P.,
1201   Jimenez, J. L., Guo, H. Y., Weber, R. J., de Gouw, J., Koss, A. R., Edgerton, E. S., Brune, W.,
1202   Mohr, C., Lopez-Hilfiker, F. D., Lutz, A., Kreisberg, N. M., Spielman, S. R., Hering, S. V.,
1203   Wilson, K. R., Thornton, J. A., and Goldstein, A. H.: Monoterpenes are the largest source of
1204   summertime organic aerosol in the southeastern United States, P Natl Acad Sci USA, 115, 2038-
1205   2043, 10.1073/pnas.1717513115, 2018.
1206

1207   Zhu, L., Jacob, D. J., Keutsch, F. N., Mickley, L. J., Scheffe, R., Strum, M., Abad, G. G.,
1208   Chance, K., Yang, K., Rappengluck, B., Millet, D. B., Baasandorj, M., Jaegle, L., and Shah, V.:
1209   Formaldehyde (HCHO) As a Hazardous Air Pollutant: Mapping Surface Air Concentrations
1210   from Satellite and Inferring Cancer Risks in the United States, Environ Sci Technol, 51, 5650-
1211   5657, 10.1021/acs.est.7b01356, 2017.
1212

1213   Zhu, L., Jacob, D. J., Kim, P. S., Fisher, J. A., Yu, K., Travis, K. R., Mickley, L. J., Yantosca, R.
1214   M., Sulprizio, M. P., De Smedt, I., Abad, G. G., Chance, K., Li, C., Ferrare, R., Fried, A., Hair, J.
1215   W., Hanisco, T. F., Richter, D., Scarino, A. J., Walega, J., Weibring, P., and Wolfe, G. M.:
1216   Observing atmospheric formaldehyde (HCHO) from space: validation and intercomparison of six
1217   retrievals from four satellites (OMI, GOME2A, GOME2B, OMPS) with SEAC(4)RS aircraft
1218   observations over the southeast US, Atmos Chem Phys, 16, 13477-13490, 10.5194/acp-16-
1219   13477-2016, 2016.
1220

1221   Ziemann, P.J., and Atkinson, R. Kinetics, products, and mechanisms of secondary organic
1222   aerosol formation. Chem. Soc. Rev., 41, 6582-6605, doi: 10.1039/C2CS35122F, 2012.
1223

Atmospheric
Chemistry
and Physics
Discussions

1224   Tables
1225
1226   Table 1. Linear regression parameters for OA vs. HCHO at low altitudes (<1 km)
1227

	US (SEAC[4]RS)	US (DC3)	US (CalNex)	South Korea (KORUS-AQ)	Wild Fires (SEAC[4]RS)	Agricultural Fires (SEAC[4]RS)	SEAC[4]RS Low NO$_2$ and Isoprene	SEAC[4]RS high NO$_2$ and Isoprene
In situ measurements OA v.s. HCHO								
Slope [a]	1.93±0.07	1.30± 0.10	1.34±0.02	2.75±0.05	25.08±0.30	3.22±0.37	1.99±0.07	1.19±0.16
Slope [b] ($\times 10^{-11}$)	9.61± 0.34	6.49± 0.49	6.66±0.09	13.71 ± 0.25	125.05 ± 1.49	16.04 ± 1.85	9.94±0.35	5.94±0.80
Intercept[c]	0.34±032	1.10±0.30	-0.90±0.06	1.36±0.22	−6.85±2.80	10.41±5.82	−0.96±0.31	1.07±1.01
Correlation coefficient r	0.59	0.76	0.88	0.70	0.97	0.85	0.64	0.44
GEOS- Chem model sampled along the flight track OA v.s. HCHO								
Slope[a]	1.25±0.03			1.39±0.05	0.48±0.05			
Slope ($\times 10^{-11}$)	6.21± 0.14			6.95± 0.23	2.37± 0.22			
Intercept	−1.32±0.11			1.88 ± 0.07	0.12±0.03			
Correlation Coefficient r	0.76			0.43	0.53			

1228
1229   [a] The unit of the slope is g g^{-1}.
1230   [b] The unit of the slope is pg molec^{-1}.
1231   [c] The unit of the intercept is μg m^{-3}.
1232   The uncertainties are one standard deviation.
1233

1234   Table 2. Methods to estimate OA surface concentrations, based on the choice of slope
1235   and intercept from a linear regression relationship between OA and HCHO data found in
1236   Table 1.
1237

1[a]	Using non-BB SEAC[4]RS relationship to represent all continental US
2[b]	Using NO$_2$ and isoprene dependent non-BB SEAC[4]RS relationship for all continental US
3	Using the CalNex LA Basin relationship for large urban cites and the non-biomass burning SEAC[4]RS relationship for other US regions
4[b]	Using the CalNex LA Basin relationship for large urban cites and the NO$_2$ and isoprene dependent non-BB SEAC[4]RS relationship for other US regions

1238

1239   [a]SEAC[4]RS was chosen to represent all continental US because it had the largest horizontal and vertical coverage.

1240   [b] In methods 2 and 4, when the product of NO$_2$ column (Sect. 2.3) and surface isoprene emission rate (Sect. 2.4) was

1241   above threshold of 5×10^{27} molec cm^{-2} atom C cm^{-2} s^{-1}, the slope and intercept from SEAC[4]RS high isoprene and NO$_2$

1242   conditions were used. When the NO$_2$ column−isoprene emission product was below that threshold, the slope and

1243   intercept from SEAC[4]RS low isoprene and NO$_2$ conditions were used. Threshold of "Isoprene × NO$_2$" is determined by

1244   its mean value over southeast US (83° - 96° W and 32° - 35°N). Large urban cities are categorized with high NO$_2$

1245   vertical columns ($>4 \times 10^{15}$ molec cm^{-2}) (Tong et al., 2015) based on the satellite NO$_2$ levels over LA. Isoprene

1246 emissions instead of concentrations are used because global models use isoprene emission inventory to simulate

1247 isoprene concentrations and isoprene emission inventory is easier to access. Since isoprene has a short-lifetime of up to

1248 a few hours (Guenther et al., 2006), the emissions have a similar spatiotemporal distribution as the concentrations.

1249

Atmospheric
Chemistry
and Physics
Discussions

1250

1251   Figures
1252
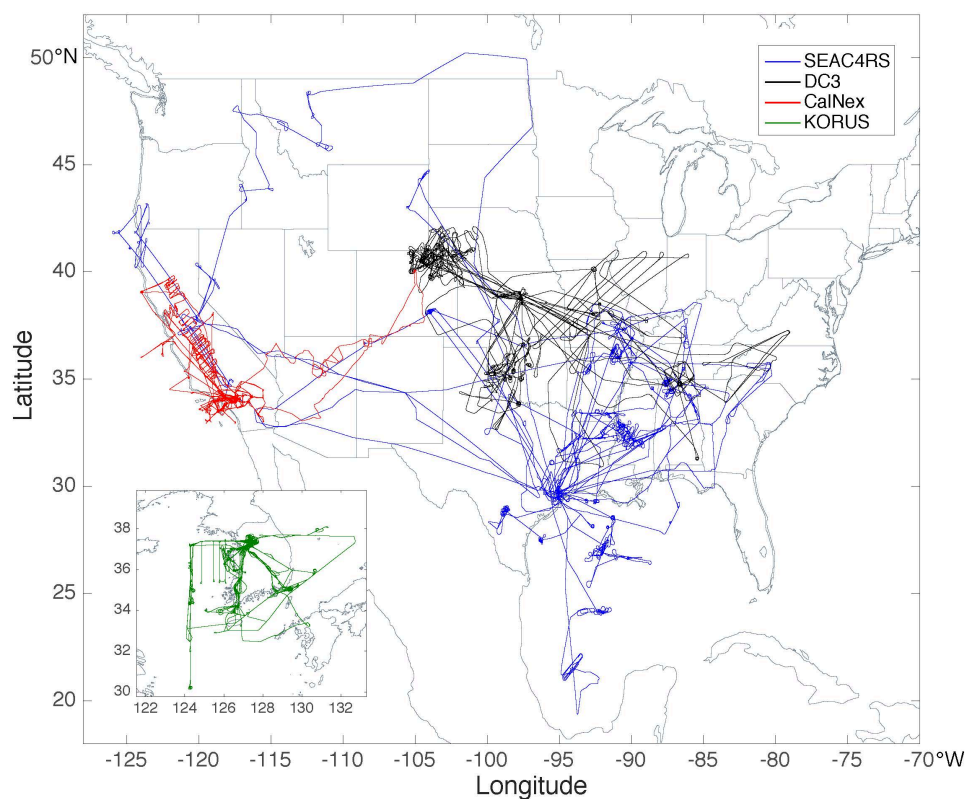
1253
1254
1255   Figure 1. Flight tracks of airborne field campaigns SEAC^{4}RS (blue), DC3 (black),
1256   CalNex (red) and KORUS-AQ (green), of which in situ OA and HCHO measurements
1257   were used.
1258
1259
1260
1261
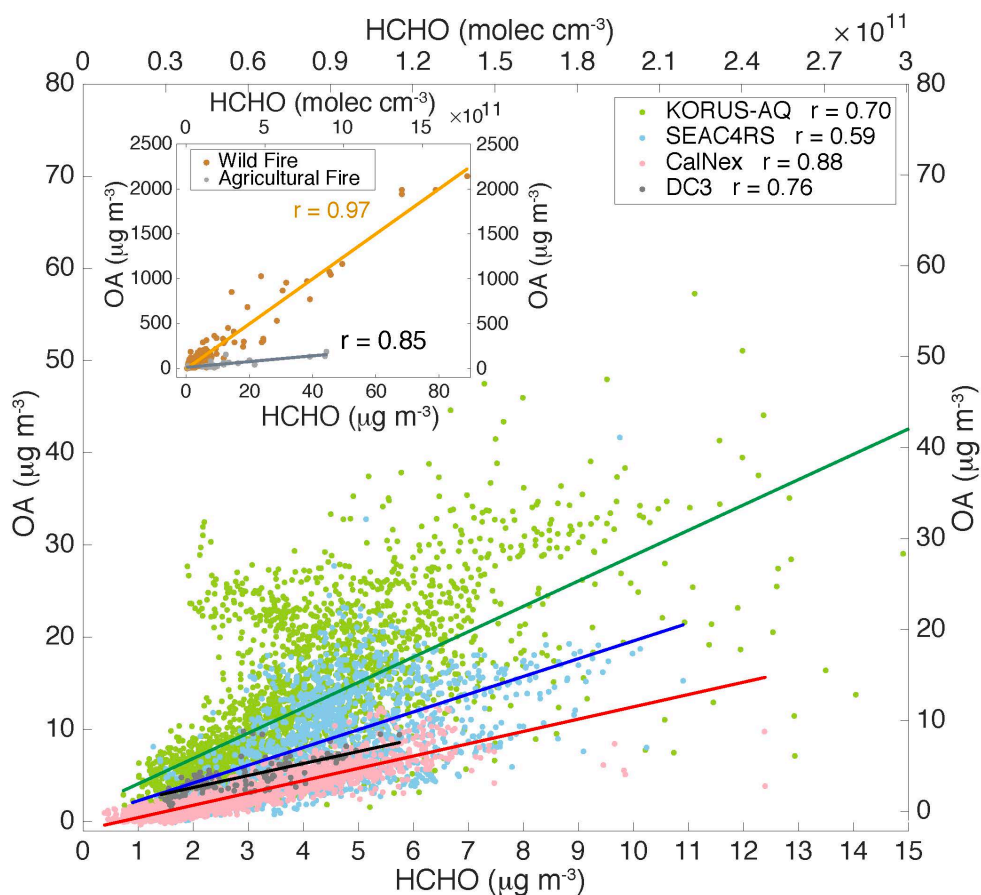
1262
1263
1264
1265
1266 Figure 2
1267 Scatter plots of in situ OA (µg m^{-3}) vs. HCHO (µg m^{-3} or molec cm^{-3}) from SEAC^{4}RS
1268 (excluding biomass burning) (blue), DC3 (dark grey), CalNex (pink), and KORUS-AQ
1269 (green) low altitude (< 1 km) data. Inset shows wildfire (brown), and agricultural fire
1270 (grey) SEAC^{4}RS data. SEAC^{4}RS biomass burning cases are defined as acetonitrile > 200
1271 pptv. The linear regression fits are shown as the darker lines and correlation coefficients
1272 are provided.
1273
1274
1275
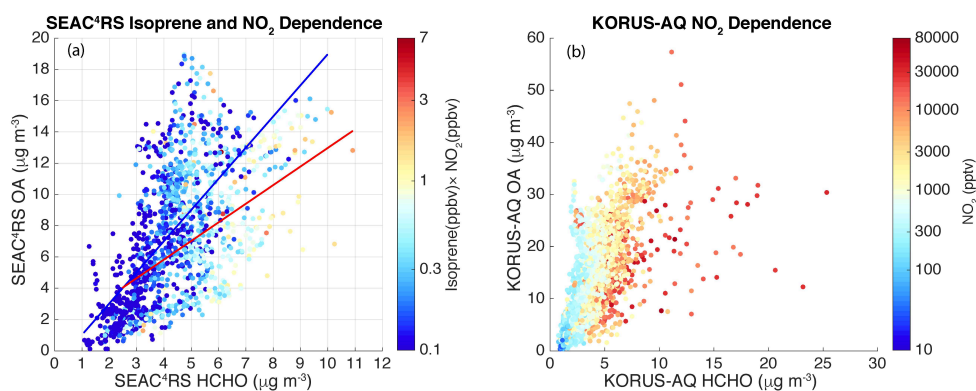
Figure 3. (a) A scatter plot of OA vs. HCHO for SEAC^{4}RS non-biomass burning low altitude data color-coded with the product of NO_2 and isoprene in log scale. The red and blue lines are the linear regression fits of high (> 0.5) and low (<0.5) product of NO_2 (ppbv) and isoprene (ppbv), respectively. (b) A scatter plot of OA vs. HCHO for KORUS-AQ data color-coded by $\log(NO_2)$.
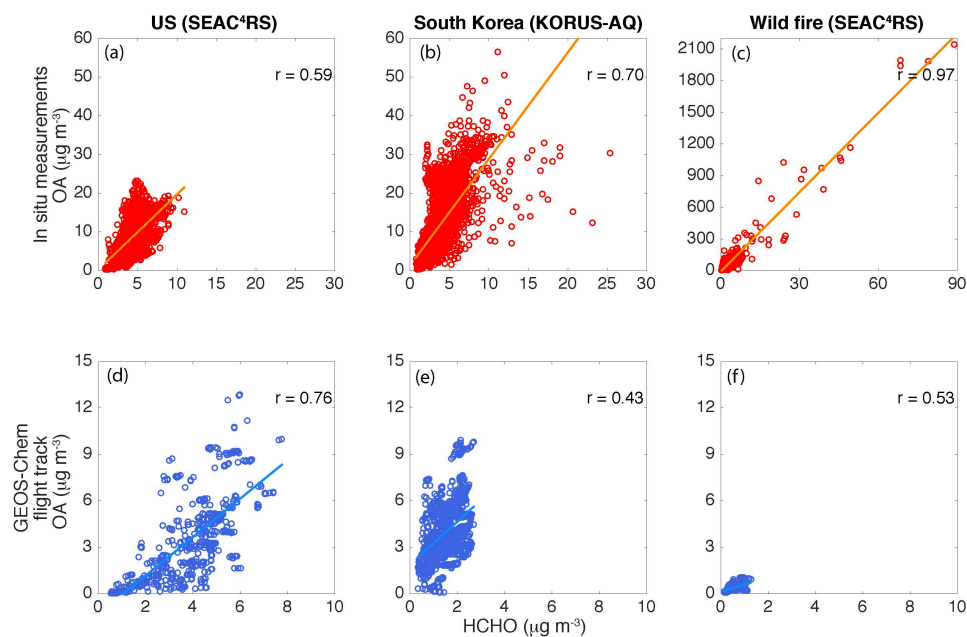
Figure 4 Scatter plots of OA vs. HCHO for US (SEAC^{4}RS altitude < 1 km non-biomass burning), South Korea (KORUS-AQ altitude < 1 km) and wildfire (SEAC^{4}RS) from in situ measurements (a, b, c) and GEOS-Chem outputs sampled along the flight tracks (d,e,f).

Atmospheric
Chemistry
and Physics
Discussions
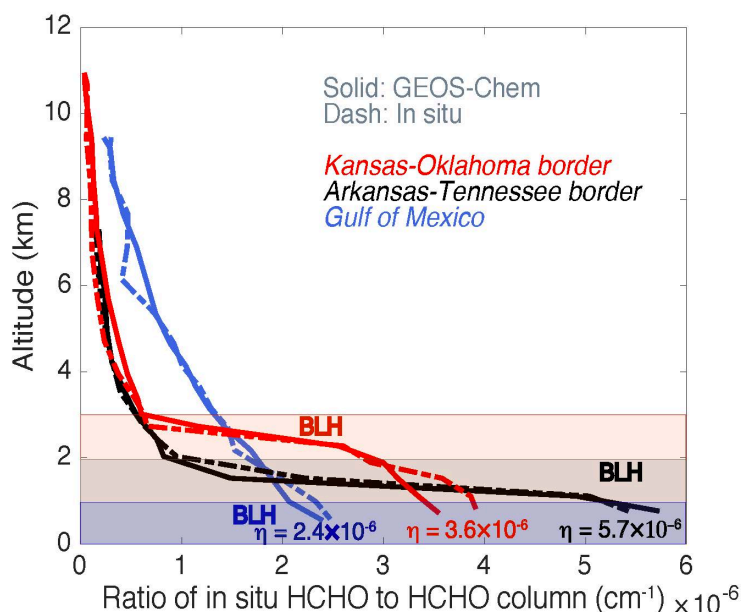
1292

Figure 5. Three typical vertical profiles of the ratio of in situ HCHO concentrations (molec cm^{-3}) to integrated HCHO column from SEAC^{4}RS flight track. These three profiles were located at Kansas-Oklahoma border (red), Arkansas-Tennessee border (black), and Gulf of Mexico (blue). Solid curves were from GEOS-Chem results and the dashed were from ISAF measurements. HCHO columns were integrated HCHO concentrations of these vertical profiles extrapolated from 0 to 10 km, assuming the HCHO below and above the measured HCHO vertical profiles were the same as the HCHO at the lowest and highest altitudes sampled, respectively. The boundary layer heights (BLH) of these three profiles were plotted by the shaded areas.
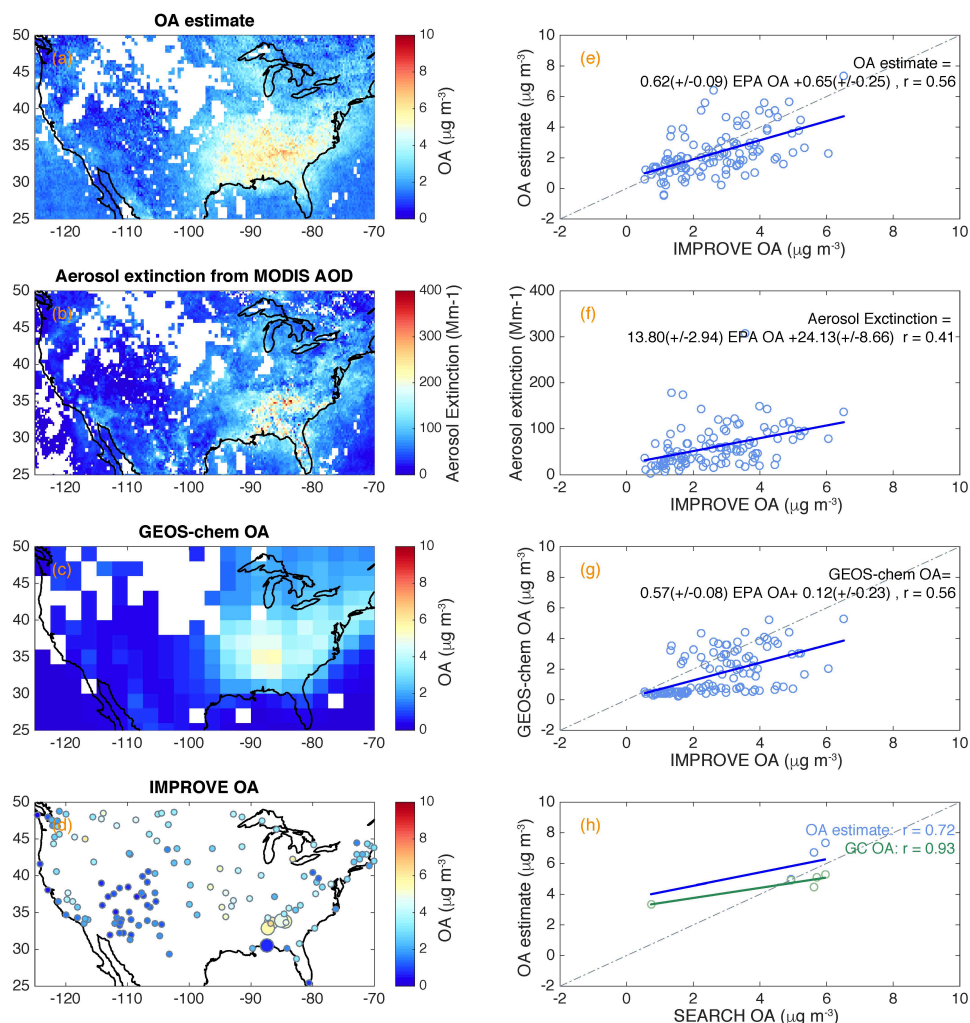
Figure 6. (a) The maps of (a) surface OA estimate (Case 1), (b) surface aerosol extinction derived from MODIS AOD, (c) GEOS-Chem simulated surface OA, and (d) EPA IMPROVE (small dots) and SEARCH (large dots) network ground sites color coded with OA concentrations for August 2013. The scatter plots of (e) surface OA estimate, (f) surface aerosol extinction derived from MODIS AOD, and (g) surface GEOS-Chem OA vs. EPA IMPROVE network ground sites OA. IMPROVE sites OA were corrected for evaporation. (h) The scatter plots of surface OA estimate and GEOS-Chem OA vs. SEARCH network ground sites OA for August 2013. GEOS-Chem OA and OA estimate did not have good correlations with SEARCH OA for other years (SI). For the scatter plots, linear regressions are shown (blue and green lines) and regression equations and correlation coefficients for the scatter plots are listed. The dashed lines in the scatter plots indicate the 1 : 1 line. Biomass burning data (UV aerosol index > 1.6) were excluded in all panels.

1319
1320
1321
1322
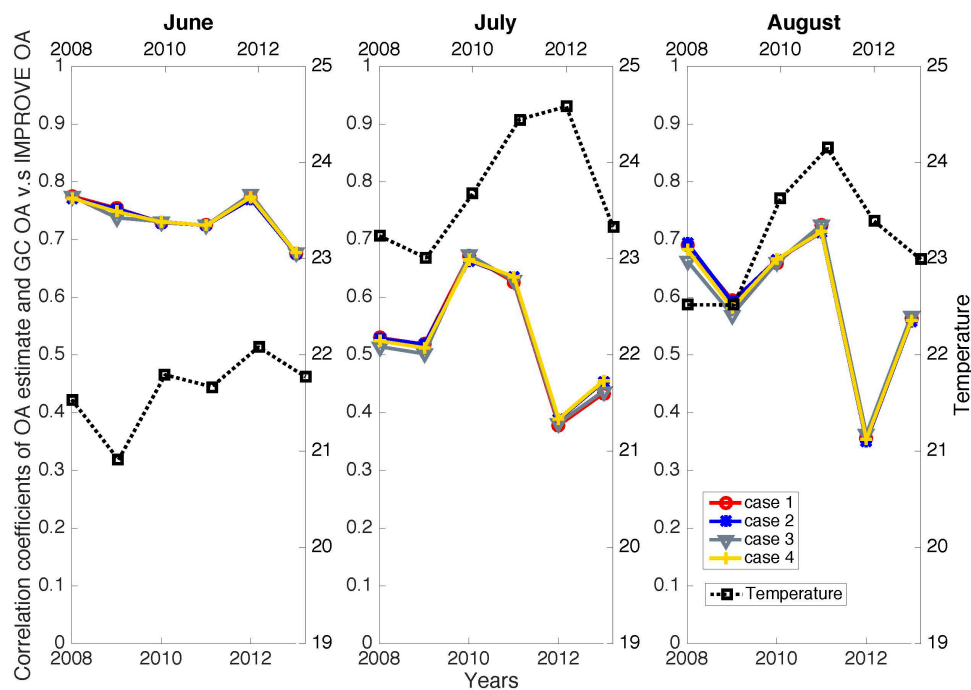
1323
1324 Figure 7. The correlation coefficients of the linear regression between the OA estimate
1325 from 4 cases (red, blue, gray, and yellow) vs. EPA-corrected OA from 2008- 2013 for
1326 June, July, and August. The monthly average ambient temperature is in black.
1327